



---

Basic Studies of Distrubted Discharge Limiters

Booske, John H.  
University of Wisconsin-Madison  
Research & Sponsored Programs  
21 N Park St STE 6401  
Madison WI 53715-1218; (680)-262-0252

---

**10-02-2014**

**Final Report**

**DISTRIBUTION A: Distribution approved for public release.**

Air Force Research Laboratory  
AF Office Of Scientific Research (AFOSR)/RTB1  
Arlington, Virginia 22203  
Air Force Materiel Command

REPORT DOCUMENTATION PAGE			Form Approved OMB No. 0704-0188		
<p>The public reporting burden for this collection of information is estimated to average 1 hour per response, including the time for reviewing instructions, searching existing data sources, gathering and maintaining the data needed, and completing and reviewing the collection of information. Send comments regarding this burden estimate or any other aspect of this collection of information, including suggestions for reducing the burden, to the Department of Defense, Executive Service Directorate (0704-0188). Respondents should be aware that notwithstanding any other provision of law, no person shall be subject to any penalty for failing to comply with a collection of information if it does not display a currently valid OMB control number.</p> <p><b>PLEASE DO NOT RETURN YOUR FORM TO THE ABOVE ORGANIZATION.</b></p>					
1. REPORT DATE (DD-MM-YYYY) 10-02-2014		2. REPORT TYPE Final Technical Performance Report		3. DATES COVERED (From - To) 1 March, 2009 - 30 November, 2013	
4. TITLE AND SUBTITLE Basic Studies of Distributed Discharge Limiters			5a. CONTRACT NUMBER		
			5b. GRANT NUMBER FA9550-09-1-0086		
			5c. PROGRAM ELEMENT NUMBER		
6. AUTHOR(S) Booske, John H.			5d. PROJECT NUMBER		
			5e. TASK NUMBER		
			5f. WORK UNIT NUMBER		
7. PERFORMING ORGANIZATION NAME(S) AND ADDRESS(ES) University of Wisconsin-Madison Research & Sponsored Programs 21 N Park St STE 6401 Madison WI53715-1218; (608)-262-0252			8. PERFORMING ORGANIZATION REPORT NUMBER		
9. SPONSORING/MONITORING AGENCY NAME(S) AND ADDRESS(ES) Air Force Office of Scientific Research 875 N Randolph St Room 3112 Arlington, VA 22203 Jennifer L. Bell (703) 696-5933 AFOSR/PKR3; USAF, AFRL DUNS 143574726			10. SPONSOR/MONITOR'S ACRONYM(S) AFOSR		
			11. SPONSOR/MONITOR'S REPORT NUMBER(S)		
12. DISTRIBUTION/AVAILABILITY STATEMENT DISTRIBUTION A: Distribution approved for public release.					
13. SUPPLEMENTARY NOTES					
14. ABSTRACT The primary objective of this AFOSR-funded consortium project is to conduct a comprehensive research investigation on distributed, self-initiated plasma discharges as candidate deployable surfaces providing counter-High-Power-Microwave (counter-HPM) capabilities. The general research goal was to achieve new physical understanding of the behavior of distributed microwave-power-limiting discharges for counter-HPM over a broad range of frequencies and radiation intensities. A second major goal of the consortium is to train outstanding students in the HPM field. The specific experimental research plan includes investigation of the effects of field enhancement structures on windows, seed electron sources, and gas ambient including pressure and species. The specific modeling research plan includes investigation of first electron effects, spatially-non-uniform microwave electric field effects, and the effects of gas ambient.					
15. SUBJECT TERMS counter-directed-energy, High Power Microwave (HPM), microwave discharge, distributed microwave limiter, metamaterial, kinetic plasma modeling					
16. SECURITY CLASSIFICATION OF:			17. LIMITATION OF ABSTRACT  UU	18. NUMBER OF PAGES	19a. NAME OF RESPONSIBLE PERSON Professor John H. Booske
a. REPORT	b. ABSTRACT	c. THIS PAGE			19b. TELEPHONE NUMBER (include area code) (608) 262-8548

Reset

Standard Form 298 (Rev. 8/98)  
Prescribed by ANSI Std. Z39.18  
Adobe Professional 7.0

# **“Basic Studies of Distrubted Discharge Limiters”**

**AFOSR GRANT FA9550-09-1-0086**

***FINAL TECHNICAL REPORT***

## **PARTICIPATING INSTITUTIONS**

MASSACHUSETTS INSTITUTE OF TECHNOLOGY  
MICHIGAN STATE UNIVERSITY  
UNIVERSITY OF MICHIGAN – ANN ARBOR  
TEXAS TECH UNIVERSITY – LUBBOCK  
UNIVERSITY OF WISCONSIN –MADISON (**LEAD**)

## **PRINCIPAL INVESTIGATOR & POINT OF CONTACT:**

PROFESSOR JOHN H. BOOSKE  
UNIVERSITY OF WISCONSIN  
ELECTRICAL AND COMPUTER ENGINEERING DEPT  
1415 ENGINEERING DRIVE  
MADISON, WI 53706  
BOOSKE@ENGR.WISC.EDU

## 1. Objectives

We completed a comprehensive research investigation on distributed, self-initiated plasma discharges as candidate deployable surfaces providing counter-HPM capabilities. The study revealed how to control and accelerate breakdown using: (1) DC voltage bias effects and seed electron sources including radioactive sources, prior breakdown discharges, UV pre-excitation/pre-ionization, VUV radiation, multipactor, and field or triple-point emission; (2) optimization of neutral gas pressure (1-760 torr) and collisionality effects and gas species (noble gases, air, and Penning gas mixtures); and (3) Metamaterials and metasurfaces. Coordinated experimental and modeling studies characterized and revealed new physical understanding of plasma filamentation, non-thermal electron energy distribution functions (EEDFs), and post-pulse recovery. Advanced experimental capabilities were developed and are ripe for exploitation for further research including: (1) methods to apply DC field bias along with intense microwave fields to window surfaces; (2) methods to exploit metasurfaces and metamaterials for enhanced control of timing and spatial distribution of breakdown; (3) microwave reflection, transmission, and scattering and CCD camera imaging diagnostics to extract rapidly varying properties of highly localized plasmas in the presence of intense HPM fields; (4) advanced OES diagnostics to extract gas and plasma temperatures, plasma densities, and non-Maxwellian EEDFs, (5) precise gas mixture control (e.g., Penning gas mixtures); and (6) seed electron source production. Advanced time-dependent multi-physics theoretical modeling capabilities were developed and are ripe for exploitation in further research of phenomena such as triple-point emission, multipactor breakdown, high pressure gas collisional discharge breakdown, field emission (including space charge limits), statistics of seed electron production, high pressure plasma filamentation, DC electric bias field effects, and electrical junction heating and electro-thermal runaway physics. Scholarship completed and recognitions acquired during the grant included 54 journal publications, 129 conference papers/presentations, and 9 prestigious awards/honors bestowed on 3 faculty with an additional 12 awards/honors for students/staff, complemented by 30 invited or award-winning talks. 48 grad students or post-docs, 8 undergrad students, and 26 faculty and staff were involved in the research sponsored in part or entirely by this grant.

## 2. Research Progress Highlights

- A comprehensive research program successfully advanced our physical understanding of microwave discharge breakdown near windows
- The study revealed the roles of an unprecedented breadth of factors related to microwave-reflecting distributed limiter breakdown (for a single research program) including:
  - Two orders of magnitude of frequency! (S-band to W-band)
  - DC voltage bias effects and seed electron sources including radioactive sources, prior breakdown discharges, UV pre-excitation/pre-ionization, VUV radiation, multipactor, and field or triple-point emission
  - Neutral gas pressure (1-760 torr) and collisionality effects and gas species (noble gases, air, and Penning gas mixtures)
  - Metamaterials and metasurfaces
  - Non-thermal electron energy distribution functions (EEDFs), and
  - Post-pulse recovery
- Advanced experimental capabilities were developed and are ripe for exploitation for further research including
  - Methods to apply DC field bias along with intense microwave fields to window surfaces
  - Methods to exploit metasurfaces and metamaterials for enhanced control of timing and spatial distribution of breakdown
  - Microwave reflection, transmission, and scattering and CCD camera imaging diagnostics to extract rapidly varying properties of highly localized plasmas in the presence of intense HPM fields
  - Advanced OES diagnostics to extract gas and plasma temperatures, plasma densities, and non-Maxwellian EEDFs
  - Precise gas mixture control (e.g., Penning gas mixtures), and
  - Seed electron source production
- Advanced time-dependent multi-physics theoretical modeling capabilities were developed and are ripe for exploitation in further research of phenomena such as
  - triple-point emission
  - multipactor breakdown
  - high pressure gas collisional discharge breakdown
  - field emission (including space charge limits)
  - statistics of seed electron production
  - high pressure plasma filamentation
  - DC electric bias field effects
  - electrical junction heating and electro-thermal runaway physics
- An incredible compilation of scholarship and recognitions including 54 journal publications, 129 conference papers/presentations, and 9 prestigious awards/honors bestowed on 3 faculty with an additional 12 awards/honors for students/staff, complemented by 30 invited or award-winning talks
- Involvement of 48 grad students or post-docs, 8 undergrad students, and 26 faculty and staff in the research sponsored in part or entirely by this grant

### 3. Research Results and Accomplishments

#### 3.1. Experimental Achievements

##### *3.1.1 Plasma structures observed in gas breakdown using a 1.5 MW, 110 GHz pulsed gyrotron*

Regular two-dimensional plasma filamentary arrays have been observed in gas breakdown experiments using a pulsed 1.5 MW, 110 GHz gyrotron. The gyrotron Gaussian output beam is focused to an intensity of up to  $4 \text{ MW/cm}^2$ . The plasma filaments develop in an array with a spacing of about one quarter wavelength, elongated in the electric field direction. The array was imaged using photodiodes, a slow camera, which captures the entire breakdown event, and a fast camera with a 6 ns window. These diagnostics demonstrate the sequential development of the array propagating back toward the source (see Fig. 1). Gases studied included air, nitrogen,  $\text{SF}_6$ , and helium at various pressures. A discrete plasma array structure is observed at high pressure, while a diffuse plasma is observed at lower pressure. The propagation speed of the ionization front for air and nitrogen at atmospheric pressure for  $3 \text{ MW/cm}^2$  was found to be of the order of 10 km/s.

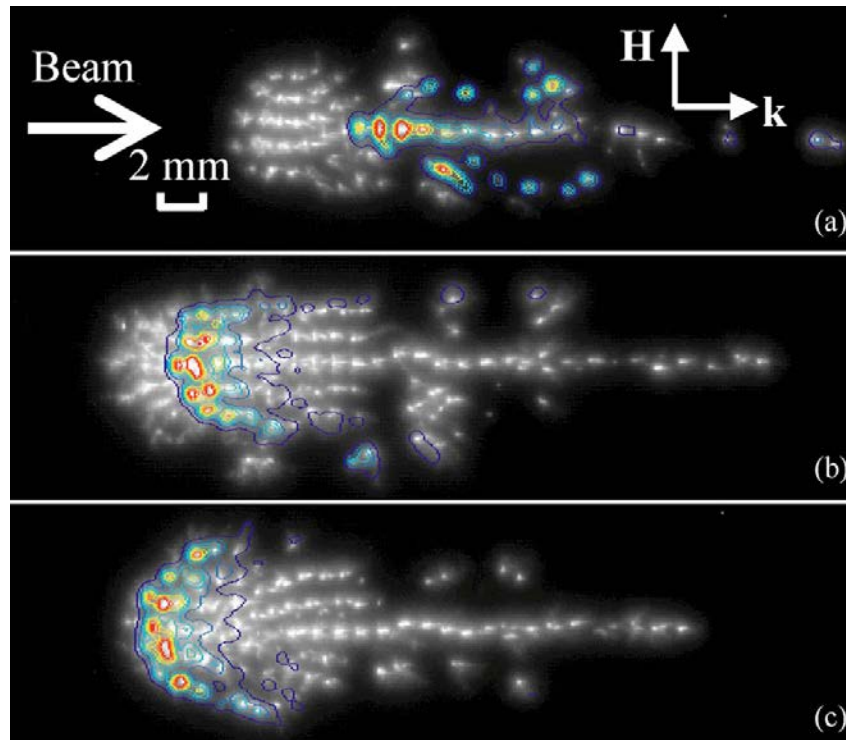


Fig. 1: Images of breakdown in ambient air at 710 Torr with 49 ns optical gate pulse starting at a)  $t=400 \text{ ns}$ , b) 1.28 microseconds, and c) 1.52 microseconds. The image is taken in the plane containing H and k, the H-plane.

### 3.1.2 Pressure dependence of plasma structure in microwave gas breakdown at 110 GHz

Our studies of 110 GHz microwave discharges in air at atmospheric pressure have demonstrated formation of a large array of quarter-wavelength-spaced plasma filaments. Our measurements show that as pressure is decreased from atmosphere to a few Torr, the discharge transitions from a well-defined array to a smeared-out array and finally to a diffuse plasma. Despite the distinct nature of breakdown phenomena at high microwave frequencies, the pressure dependence of the breakdown threshold field is seen to follow a Paschen-type curve (see Fig. 2). Data for air and argon at 110 GHz are compared with previous low-frequency data.

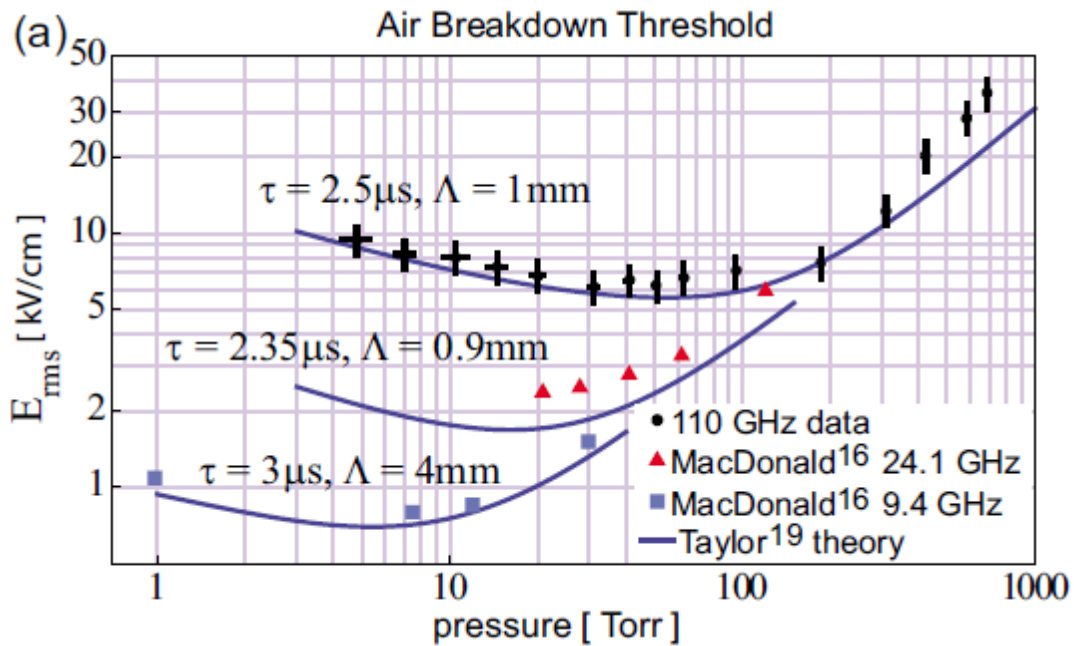


Fig.2 Breakdown threshold field vs pressure. Air data: 110 GHz (circles), MacDonald 24.1 GHz triangles, MacDonald 9.4 GHz squares, Taylor model curve.

### 3.1.3 Measurements of Electron Avalanche Formation Time in W-Band Microwave Air Breakdown

We have measured the formation times of electron avalanche ionization discharges induced by a focused 110 GHz millimeter-wave beam in atmospheric air. Discharges take place in a free volume of gas, with no nearby surfaces or objects. When the incident field amplitude is near the breakdown threshold for pulsed conditions, measured formation times are 0.1–2 microseconds over the pressure range 5–700 Torr (see Fig. 3). Combined with electric field breakdown threshold measurements, the formation time data shows the agreement of 110 GHz air breakdown with the similarity laws of gas discharges.

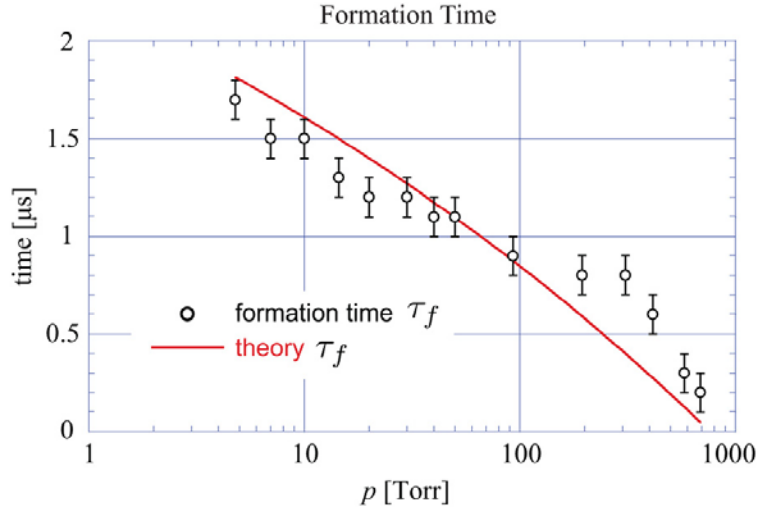


Fig. 3 Measured formation time (open circles) versus pressure.

### 3.1.4 Observation of plasma array dynamics in 110 GHz millimeter-wave air breakdown

We have made dynamical measurements of self-organizing arrays of plasma structures in air induced by a 110 GHz millimeter-wave beam with linear or circular polarization. The formation of the individual plasmas and the growth of the array pattern are studied using a fast-gated (5–10 ns) intensified camera (see Fig. 4). We measure the time-dependent speed at which the array pattern propagates in discrete steps toward the millimeter-wave source, observing a peak speed greater than 100 km/s. We observe the expansion of an initially spherical plasma into a disk or an elongated filament, depending on the polarization of the incident beam. The results show good agreement with one-dimensional ionization-diffusion theory and two-dimensional simulations.

### 3.1.5 Spectroscopic Temperature Measurements of Air Breakdown Plasma Using a 110 GHz Megawatt Gyrotron Beam

Temperature measurements are presented of a non-equilibrium air breakdown plasma using optical emission spectroscopy. A plasma is created with a focused 110 GHz 3 microsecond pulse gyrotron beam in air that produces power fluxes exceeding  $1\text{MW}/\text{cm}^2$ . Rotational and vibrational temperatures are spectroscopically measured over a pressure range of 1–100 Torr as the gyrotron power is varied above threshold. The temperature dependence on microwave field as well as pressure is examined. Rotational temperature measurements of the plasma reveal gas temperatures in the range of 300–500 K and vibrational temperatures (see Fig. 5) in the range of 4200–6200 K. The vibrational and rotational temperatures increase slowly with increasing applied microwave field over the range of microwave fields investigated.

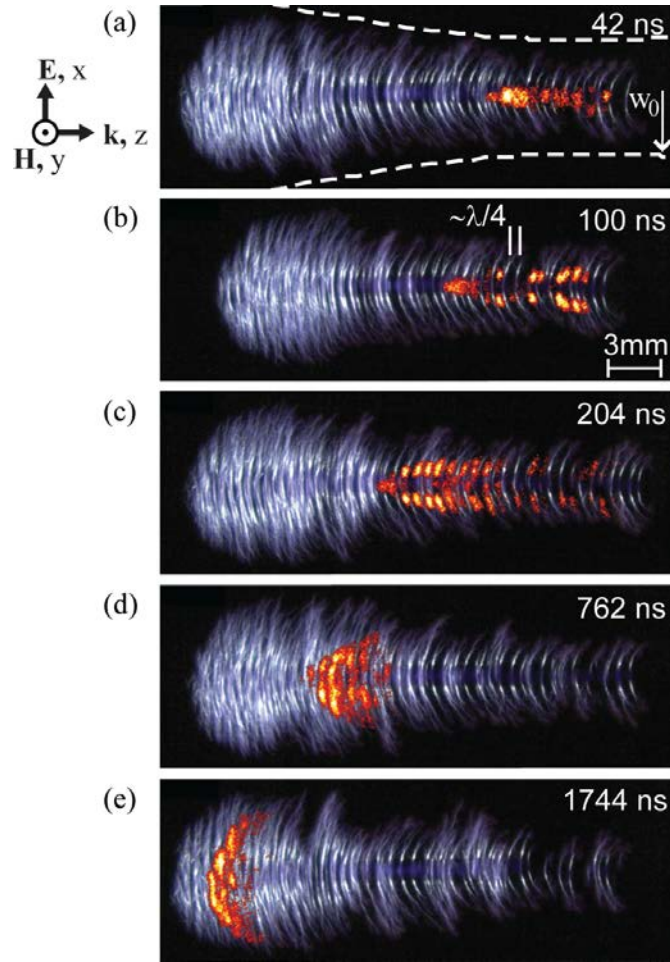


Fig. 4 Open-shutter (background image, blue) and fast-gated (overlay, orange) photographs of breakdowns with linearly polarized beam.

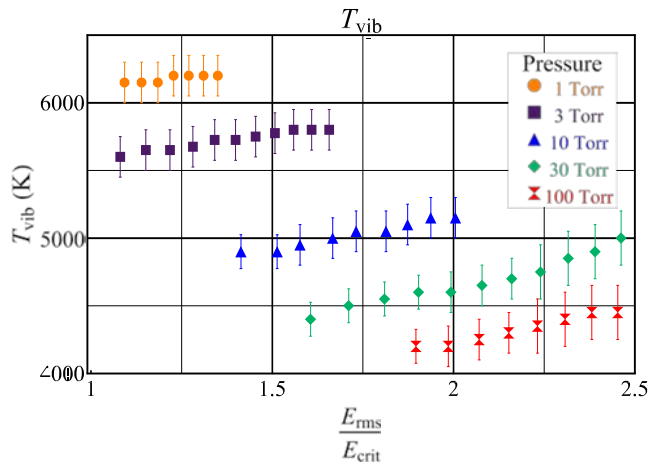


Fig. 5 Measured  $T_{vib}$  as a function of applied microwave electric field for five different pressures by comparing nitrogen vibrational band-heads at 353.7 nm and 357.7 nm with SPECAIR code.

### 3.1.6 Millimeter wave scattering and diffraction in 110 GHz air breakdown plasma

We have made measurements of the scattering, reflection, absorption, and transmission of a 1.5MW, 110 GHz quasioptical gyrotron beam by a self-induced air breakdown plasma. The breakdown forms a periodic array of plasma filaments, oriented parallel to the incident electric field polarization that propagates toward the microwave source. For incident intensity of  $3 \text{ MW/cm}^2$ , calorimetric measurements show that as much as 45% of the full beam power is absorbed by the plasma, averaged over the pulse, 1% is reflected backward, and the remainder is transmitted and also scattered into a wide angular spread. We observe that approximately 10 times more power is scattered in the direction perpendicular to the filaments than parallel. The far-field angular distribution of transmitted power exhibits a diffraction pattern that changes throughout the 2 microsecond life of the plasma.

### 3.1.7 Vacuum Ultraviolet emission from pulsed discharges at atmospheric pressure.

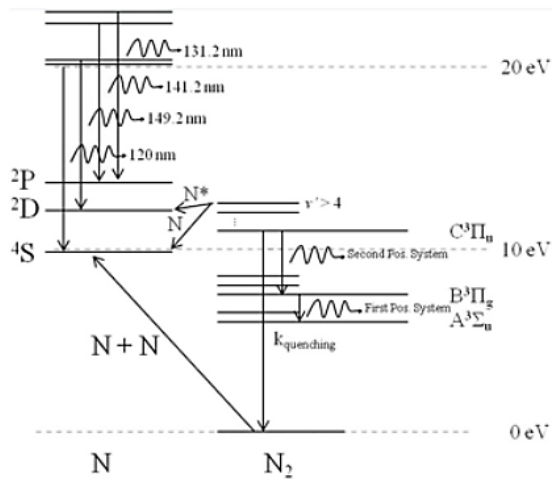


Fig. 6. Energy level diagram for molecular and atomic species of nitrogen showing processes of interest [1].

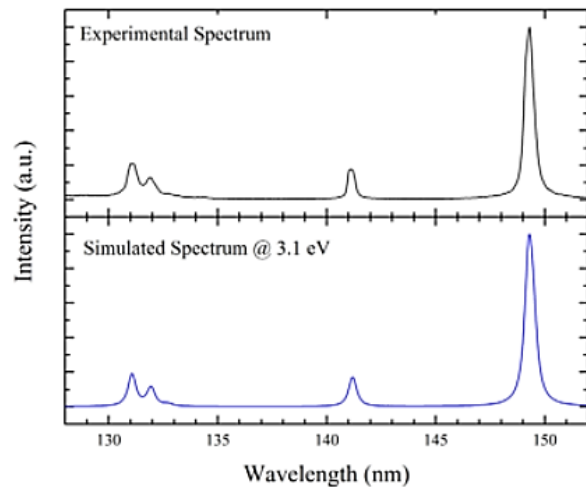


Fig.7. Experimental and simulated spectrum of atomic nitrogen emission between 130 and 150 nm [1].

The optical emission from a developing low-temperature plasma in nitrogen gas in the VUV–VIS regimes has been characterized. A locally developed software package was utilized to determine the temperature of the developing plasma assuming the excited state population is Boltzmann distributed, see Fig. 6 for primary atomic nitrogen levels considered. Time-resolved emission spectroscopy in the VUV region revealed a non-Boltzmann distributed population before voltage collapse which transitioned into a Boltzmann distributed population with an electronic temperature of 3.1 eV. Further investigation of the UV regime indicated the dominant presence of the molecular nitrogen second positive system. Since emission from atomic nitrogen appears later than the emission from nitrogen molecules, a two-step process is believed to be the leading mechanism for the generation of excited atomic nitrogen. First, dissociation of nitrogen molecules occurs due to electron impact, which is then followed by a second electron collision that results in excitation of the dissociated nitrogen, followed by spontaneous emission of VUV radiation. After voltage collapse, the increase in current, and thus electron density, leads to the continuous emission of atomic and molecular emission even though the applied field is collapsed

across the gap. More details available in ref. [1], which also contains a detailed description of the utilized spectral simulation software, SPECTRAPLOT.

### 3.1.8 Non-intrusive diagnostic method for dissociation degree in pulsed discharges

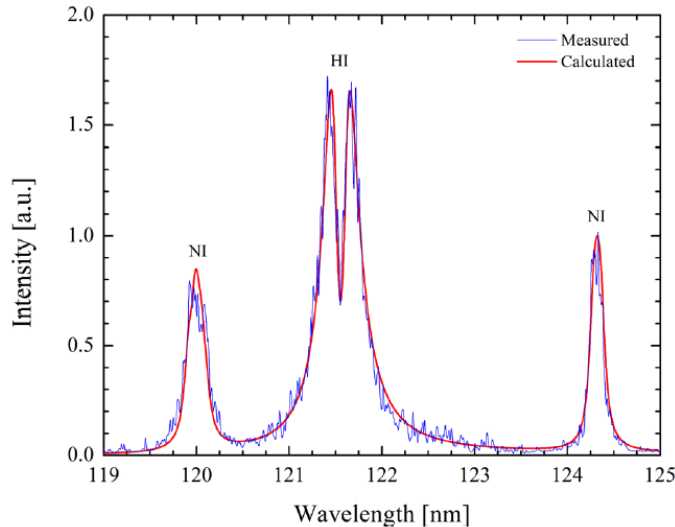


Fig. 8. Comparison of measured (blue) and calculated (red) profiles for N and HI emission observed from the early spark phase of plasma formation in 80%/20%  $N_2/H_2$  mixture by volume at atmospheric pressure (exposure time - 100 ns). The Lorentzian and rectangular components due to instrumentation are 0.097nm and 0.097 nm, respectively [2].

We demonstrated a method for determining the dissociated density of H atoms in  $H_2$  plasmas by measuring the absorption characteristics of the  $2p \rightarrow 1s$  Lyman- $\alpha$  transition of H at 121.57 nm [2]. This transition has been measured previously to determine dissociated gas density, but only at the expense of using an invasive radiation source, such as a micro-discharge hollow cathode lamp, to provide external photons for absorption in the plasma medium. This approach has the drawback of introducing a large flux of high energy VUV radiation into the plasma environment, which has the ability to directly dissociate molecules via single photon absorption. The method presented in this paper instead uses the intrinsic self-radiation released from the plasma spark, which undergoes partial radiation trapping as it leaves the plasma medium. Sufficient levels of self-emission at 121.5 nm are detected, leading to a treatment of H selfabsorption as an estimate of dissociated gas density. The plasma state is preserved without alteration by external radiation sources in the experiment, and the H emission has the added benefit of providing information on the electron density derived from measuring the Stark broadened line profile. If a  $N_2/H_2$  mixture is used, the self-absorption approach can be extended to simultaneously provide information on the density of N atoms by comparing the absolute intensity of H radiation to N radiation at 124.3 nm, in addition to measuring the approximate absorption characteristics of the  $2s^2 2p^2 3s \rightarrow 2s^2 2p^3$  transition(s) of ground state N at 119.96 nm, 120.02 nm, and 120.07 nm. It is worth noting that the self-absorption treatment could also be used to determine dissociated O density of air plasmas in the future, by using the  $2s^2 2p^3 3s \rightarrow 2s^2 2p^4$  transition of O.

### 3.1.9 Post Pulse Recovery of plasma for microwave transmission

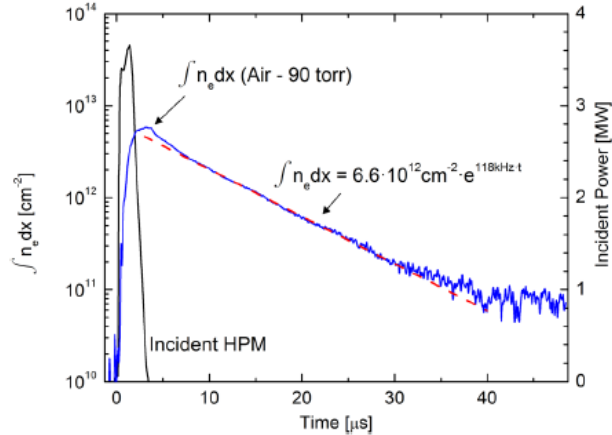


Fig. 9. Longitudinal integral of the electron density (log) vs. time (linear) for 90 torr in air shows a linear slope of -118 kHz, which corresponds to the reaction rate of  $O_2$  attachment. [3]

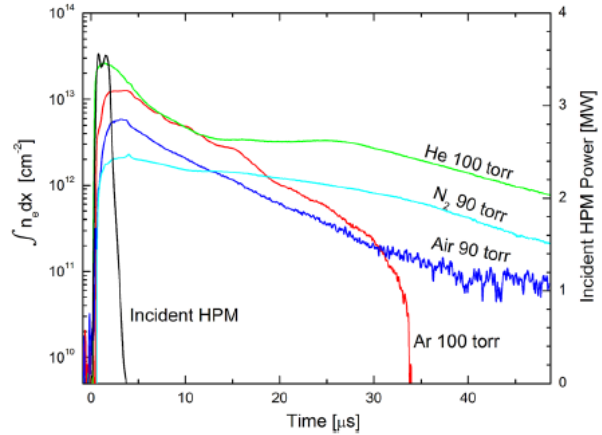


Fig. 10. Comparison of the electron density evolution for the 4 gases measured at 90–100 torr. [3]

It was demonstrated that for low temperature plasma in an air environment at 90 torr, the dominant electron loss process is 3-body attachment [3]. Due to this being the lowest term of electron density in the continuity equation, one concludes that this reaction will dictate the lifetime of the plasma ( $\sim 20 \mu\text{s}$  per decade, cf. Fig. 9, leading to  $\sim 200 \mu\text{s}$  plasma lifetime). For  $N_2$ , the relaxation of the plasma at early times is dominated by 2-body recombination and is consistent across the pressure range of 60–145 torr. For helium, the relaxation is rather complex (four independent mechanisms with two different exponential terms of the electron temperature). For this, detailed knowledge of the electron temperature is needed to validate the model. Under the assumption that the developed model model is valid, the temperature can be seen to drop from 600 K to 375 K in a matter of 12  $\mu\text{s}$ , which is similar to the cooling rates reported elsewhere. In argon, the EEDF deviates from Maxwellian and energy exchange between the electrons and metastables causes the transmitted power to oscillate low pressures ( $\sim 10$  torr). This is caused by either (or combination thereof) the fluctuations of the EEDF (i.e., collision frequency) or the electron density itself.

### 3.1.10 Pulsed VUV microhollow cathode discharge with > 1 W average output

Utilizing a short pulse, high current excitation at MHz repetition rate the overall electrical input power to the microhollow cathode discharge, MD, was significantly increased all the while maintaining stable operation. In addition, the VUV yield efficiency as well as the absolute VUV power output was increased by as much as three orders of magnitude for the latter. The Ar- $H_2$  gas mixture was found to be less susceptible to impurities and hydrogen Lyman- $\alpha$  emission remained dominant in the VUV regime. A MD-VUV source with a time averaged power just below 3.4 watts, with peak power in excess of 42.8 W was reported, see Fig. 11. These results suggest that additional studies with repetitively pulsed gas mixtures other than the presented may yield even higher power MD output in the VUV.

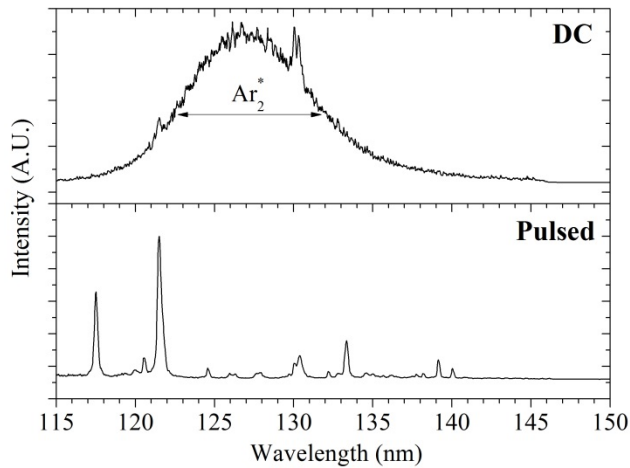


Fig. 11. (a) Experimental argon spectrum produced by a 1.04 W (5 mA) DC excitation showing  $\text{Ar}_2^*$  excimer emission. (b) Experimental argon spectrum produced by a 567 W input pulsed excitation

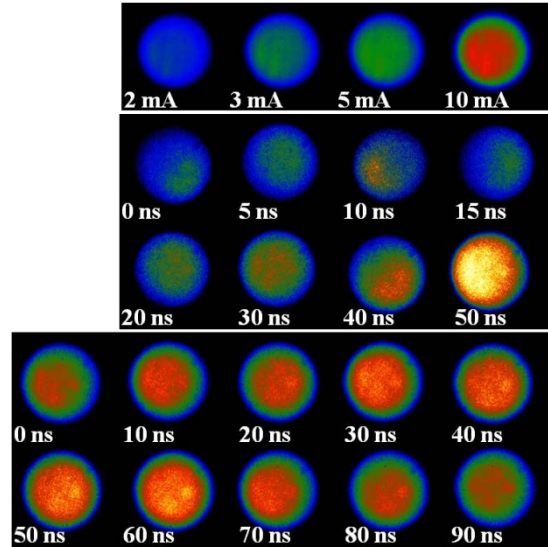


Fig. 12: High speed images of the MD for DC excitation, initial pulse, and 100<sup>th</sup> pulse.

The top set of images in Fig. 12 was taken of a DC discharge for comparison. The second set of images was of the discharge during the initial pulse, and the third set were images over the 100th pulse (note that each set has different camera setting thus the color scales do not correlate). It is demonstrated that, even when in arc operation, the discharge remains stable. Additional images not included show a dim glow from the MD well beyond 1  $\mu\text{s}$  after the previous pulse. With this it is reasonable to assume that a background density remains in the MD as an initial condition for the subsequent pulse, enabling a more rapid transition to arc operation. It is planned to utilize the VUV generating MD as pre-ionization source for HPM discharges. Adjusting the power would enable adjusting the delay of the HPM breakdown.

### 3.1.11 Seed electron generation methods

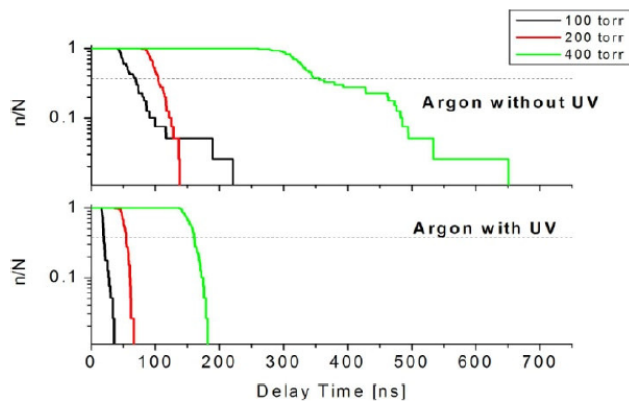


Fig. 13. Laue plot of statistical waiting times for breakdown after pulse application showing the distributions of delay times for 3 pressure values without and with UV [5].

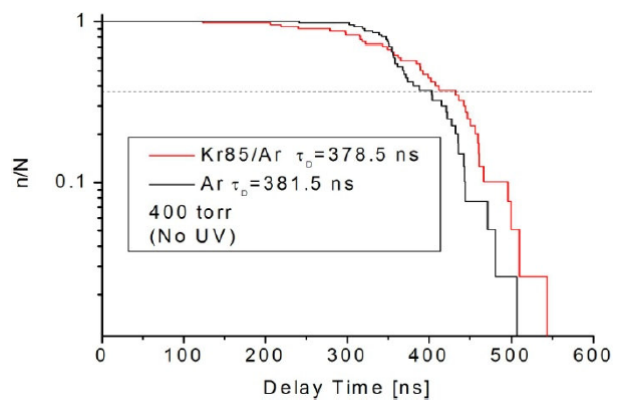


Fig. 14. Laue data for Kr85/Ar and Ar with the average delay times indicated[5].

Radiation was used as a source for providing seed electron density sufficiently large to attempt eliminating the statistical waiting time for HPM surface flashover initiation at 2.85 GHz frequency and 4 MW power levels. It was estimated that the utilized UV illumination (comparable to levels the sun provides on a “sunny day”) provided a sufficient number or density of electrons, showing a drastic influence on the delay times and delay time distributions, see Fig. 13. It is still difficult to quantify this initial density from the UV illumination due to the complication caused by the presence of the polycarbonate surface and corresponding charge trapping/discharge mechanisms. To further help establish a better idea of this initial contribution in the future, experiments are planned with varied UV power densities allowing for a clearer picture of this initial electron density contribution. This “high intensity” UV illumination does not eliminate all statistical variations. Fluctuations in the amplification process and variations of the experimental conditions (magnetron output waveform and influence of switching/pulse forming plasma) contribute about equal parts of the fluctuations, with typical widths of the delay time distributions of several nanoseconds. While the ionizing capabilities of Kr85/Ar are poor, see Fig. 14, radioactive isotopes are still capable of being able to produce sufficient ionization events. A better approach might be to use an emitting isotope with much shorter absorption length and higher ionization capability.

### 3.1.12 Impact of strong DC field on HPM breakdown

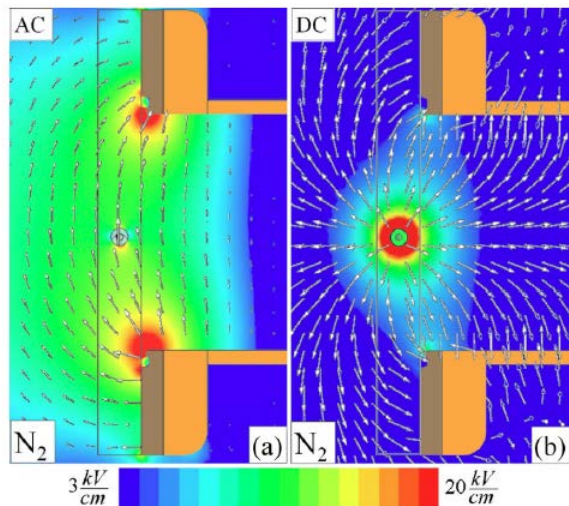


Fig. 15. Electric field due to (a) rf excitation at a phase with maximum field at the output window. The field direction is reversed 180° later; (b) dc excitation, positive voltage polarity. The microwave radiation propagates from right to left through a dielectric window from vacuum into a nitrogen environment [6].

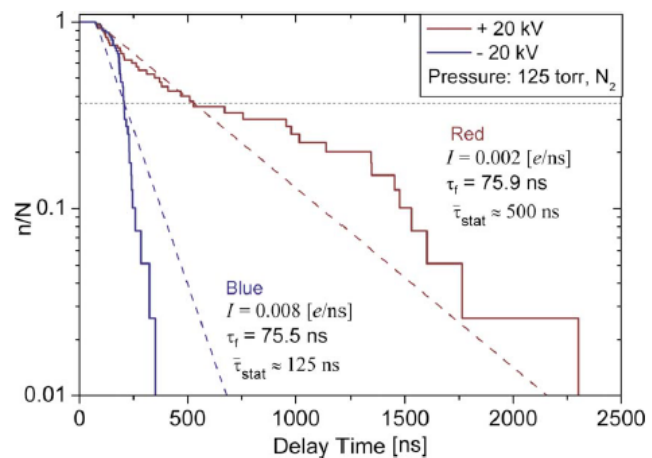


Fig. 16. Statistical breakdown data from electrode with +20 kV (red), the electrode with -20 kV (blue) [6]

Experimental data for high power microwave-induced surface flashover with the introduction of a dc electric field, see Fig. 15, has demonstrated that the statistical waiting time and the formative time are significantly affected with the introduction of positively or negatively polarized dc electric field, see Fig. 16. We conclude from the experimental data that a strong

external dc field will contribute to the ionization of the gas in the test chamber indicated by the observed reduction in formative delay time. The distinct dependence of the statistical delay time on the dc field polarity seems consistent with free electrons from detachment processes being the primary breakdown initiating species. Future research will evaluate gases with electron attaching properties.

### 3.1.13 Metamaterial for breakdown delay adjustment

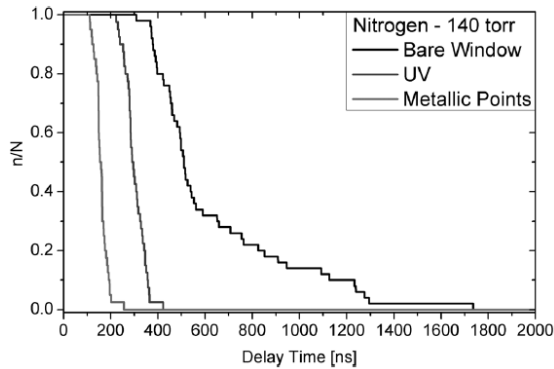


Fig. 17. Experimental delay time distribution of the bare window (black curve), UV illuminated window (dark gray curve), and window with metallic points (light gray curve) [7].

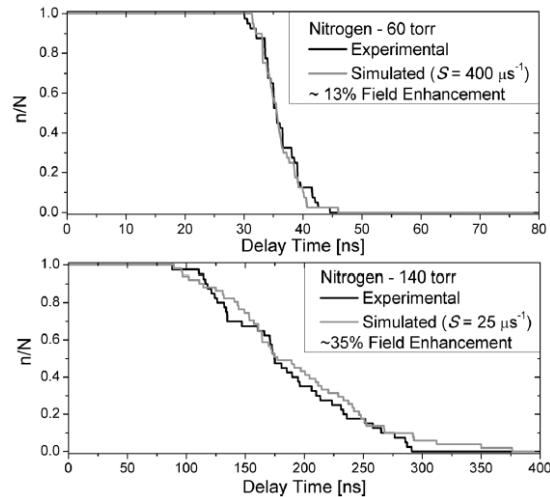


Fig. 18. Measured and simulated HPM flashover statistics; model (gray curve) and experimental (black curve) data for nitrogen at 60 and 140 Torr, metallic points, no UV [7].

Accurate statistical modeling of delay times for HPM surface flashover initiation was demonstrated for an experiment for a simple metamaterial structure in which metallic field enhancements were deposited in a onto a dielectric surface [7]. It was shown that the probability to find  $n$  electrons in a discharge is based on the exponential distribution, which is then integrated in order to determine the probability of no surface flashover. Initial electron generation rates were estimated for pressures of 60–140 Torr in nitrogen. The generation rates, combined with an exponential distribution, effectively model the probability for no flashover for various environments and have proven to be pressure dependent. These rates have been quantified for the various pressures in nitrogen based on the statistical model and the overall distribution of experimental delay times. Choosing pressure or the metamaterial’s microdot sizes enables adjusting the observed breakdown delay times and breakdown power.

- [1] A. Fierro, G. Laity and A. Neuber, “Optical emission spectroscopy study in the VUV–VIS regimes of a developing low-temperature plasma in nitrogen gas” *J. Phys. D: Appl. Phys.* 45, 11 pages, (2012).
- [2] G. Laity, A. Fierro, J. Dickens, A. Neuber, and K. Frank, “Simultaneous measurement of nitrogen and hydrogen dissociation from vacuum ultraviolet self-absorption spectroscopy in a developing low temperature plasma at atmospheric pressure,” *Appl. Phys. Letters*, 102, 184104, (2013).

- [3] S. Beeson, J. Dickens, and A. Neuber, "Plasma relaxation mechanics of pulsed high power microwave surface flashover," *Physics of Plasmas* 20(9), 093509 - 093509-9 (2013).
- [4] J. Stephens, A. Fierro, B. Walls, J. Dickens, A. Neuber, "Nanosecond, repetitively pulsed microdischarge VUV source," to be submitted, Feb. 2014.
- [5] M. Thomas, J. Foster, H. Krompholz, A. Neuber, "Use of Radiation Sources to Provide Seed Electrons in High Power Microwave Surface Flashover," *Proceedings of the 2009 IEEE Pulsed Power Conference (PPC)*, pp. 124-128, Washington, DC, June 2009.
- [6] J. Foster, M. Thomas, A. A. Neuber, "Variation of the statistical and formative time lags of high power microwave surface flashover utilizing a superimposed DC electric field," *J. Appl. Phys.* 106, pp. 063310-063310-4 (2009).
- [7] J. Foster, H. Krompholz, and A. Neuber, "Statistical analysis of high power microwave breakdown surface flashover delay times in nitrogen with metallic field enhancements," *Phys. Plasmas* 18, 113505, (2011).

### 3.1.14 Effects of DC electric field on window breakdown

#### Introduction

The goal of this work was to design and demonstrate a microwave window with a tunable power threshold for signal transmission. Such a window would be transparent to powers below the threshold, whereas higher powers would initiate rapid surface breakdown and subsequent blockage microwaves.

The approach investigated (at UM) is somewhat unusual in that the formation of a multipactor discharge is encouraged. Multipactor is a rapid electron multiplication phenomenon that may quickly block HPM by quickly developing a large electron population near the window surface, which then ionizes the background gas to form a plasma. The collective behavior of the plasma can then absorb or reflect the incident microwaves.

#### Theory

The theoretical basis for this work is discussed in section 3.2.

#### Experiment Configuration

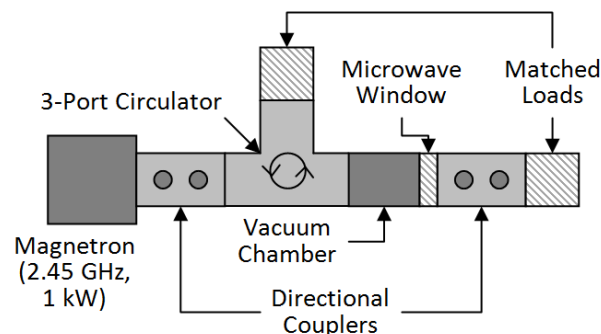


Figure 19: Experiment configuration.

A graphical depiction of the experimental configuration can be seen in Fig. 19. The window material was Lexan, which has a relatively low secondary electron yield  $\delta \approx 2.5$ . The RF source was a 2.45GHz, 0.2-1.0kW CW magnetron intentionally limited to the minimum output power of 200W to avoid damaging the window. The rise time was 200ms, which was long enough to preclude reliable timing measurements. Instead, the goal of this initial experiment was to determine if the DC bias had any effect whatsoever on window breakdown. The background gas was argon, and the pressure range was a relatively broad 50mTorr to 75 Torr.

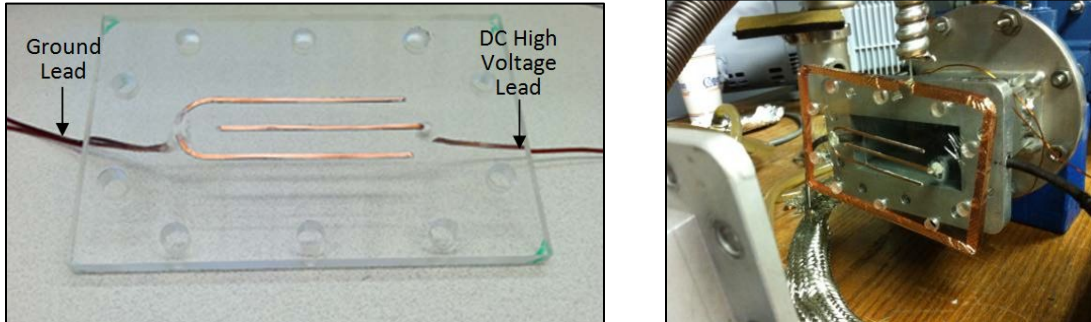


Figure 20: (Left) Lexan window with embedded conducting network. (Right) Window mounted between two WR284 waveguide flanges.

Fig. 20 shows the Lexan window with the embedded conducting network. The central conductor is brought to high negative voltage with respect to the grounded outer conductors. The conductors are on the low pressure side, which provides a large triple point area to provide a source of seed electrons, which are critical for initiating a multipactor discharge. The window is mounted between two WR284 waveguide flanges. The surrounding copper tape prevented RF from leaking into the lab and provided electrical continuity between the waveguides. Maximum power transmission was approximately 85%, which was sufficient for the experiment. Diagnostics included measurement of the DC voltage and current, incident and transmitted RF power, and an optical fiber and PMT to detect the presence of a glow discharge.

### Experiment Findings

Preliminary results were collected using low-pressure air. These results showed high variability, which motivated the use of argon to improve repeatability. However, the use of argon necessitated the use of pressures greater than 14Torr. This is because 200W of RF power alone was sufficient to break down lower pressures, whereas very low pressures not subject to immediate breakdown (generally less than 50mTorr) were an argon/air mixture due to inherent leaks in the experimental setup. While volumetric ionization is expected to dominate surface multipactor at these higher pressures, results were nonetheless encouraging.

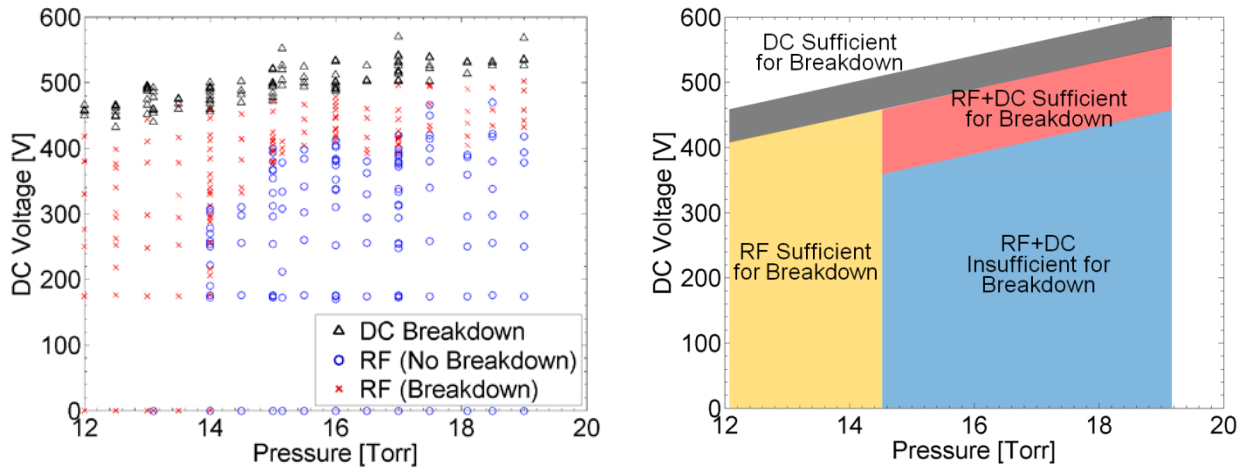


Figure 21: (Left) Experimental results using argon and 200W RF power. (Right) Conceptual illustration of the different operational regions.

Fig. 21 shows some of the experimental results. The left plot identifies the outcome of several trial shots, and the right identifies the different regions of operation based on the results on the left. Pressures below 14Torr can be ignored because, as previously stated, the 200W of RF power initiates breakdown with zero DC bias. The other points can be interpreted as follows: At a fixed pressure, some DC bias below the DC breakdown threshold is applied to the conducting network. The window is then illuminated with 200W of RF power for two seconds. If breakdown occurred, the point is marked as a red X, otherwise a blue circle was used.

Of particular note is the region designated by the red band where the 200W, in conjunction with the DC bias, was sufficient to initiate breakdown. In the absence of the DC bias, the 200W was insufficient, which shows that the window functioned successfully as a power-tunable microwave limiter.

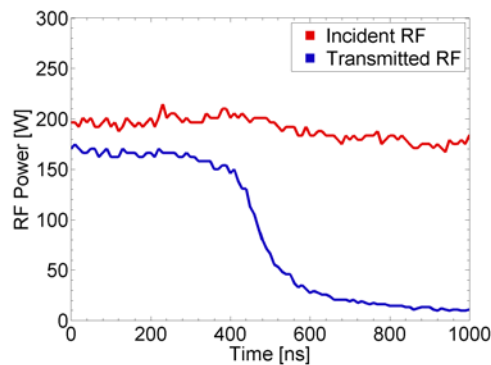


Figure 22: Diode responses for RF-initiated breakdown in 50 mTorr argon.

A significant side-effect of operation at higher pressures is the localized formation of plasma on the window. As shown by Fig. 22, breakdown at low pressures ( $< 1$ Torr) leads to smooth, substantial elimination of transmitted power (as little as -20dB transmitted power). At higher pressures, particularly those above 25Torr, breakdown is frequently observed in discrete steps. The left traces shown in Fig. 23 illustrate this effect. This is thought to be due to highly localized plasma formation at different locations on the window. Another observation at higher pressures is the random increase in transmitted power through the window after breakdown occurred. This

can be seen from the traces shown on the right plot of Fig. 23. Again, this is thought to be due to localized plasma patches that occasionally extinguish as the RF bends around the plasma, which then form again later in time.

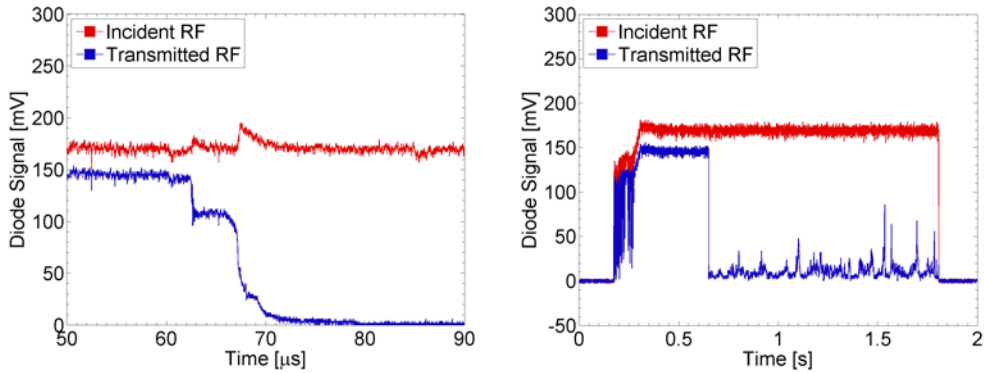


Figure 23: Diode responses for RF-initiated breakdown in 75 Torr argon.

Justification for this reasoning stems from direct observations of DC discharges on the window. Two examples are shown in Fig. 24. Low pressures exhibit a uniform glow discharge across the conducting network, whereas higher pressures exhibit considerable filamentation and localization. This is one possible explanation for the greater consistency observed at lower pressures between 14 Torr and 25 Torr as compared to pressures between 25 Torr and 75 Torr.

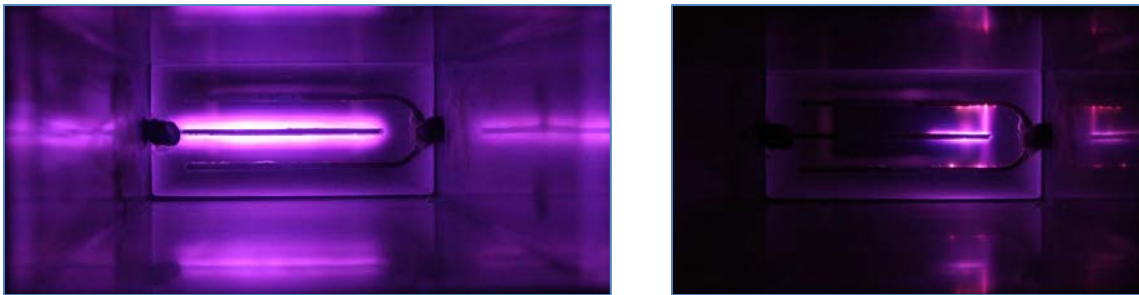


Figure 24: (Left) DC discharge at 300 mTorr. (Right) DC discharge at 19 Torr.

A final observation was the gradual degradation of performance over time as measured by consistency and repeatability of results. After extensive testing, the window was inspected and found to have a significant amount of contaminants on the surface. These are thought to be due to plasma-induced chemistry with the window material.

### Ongoing Work

Based on the initial experiment, there are several goals for ongoing work. Measurement of RF extinction times is of significant interest, which necessitates the use of a pulsed source with fast rise-time. The impact of different secondary electron yields is also of interest, particularly materials with high yields that are also resistant to plasma-induced surface degradation. Finally, the target pressure range is between 50-500mTorr to reduce plasma localization and operate in a multipactor-dominant regime. Operation in this pressure range therefore requires RF powers below 200W at 2.45GHz to avoid immediate RF breakdown. There is some interest in the effects of different frequencies as well.

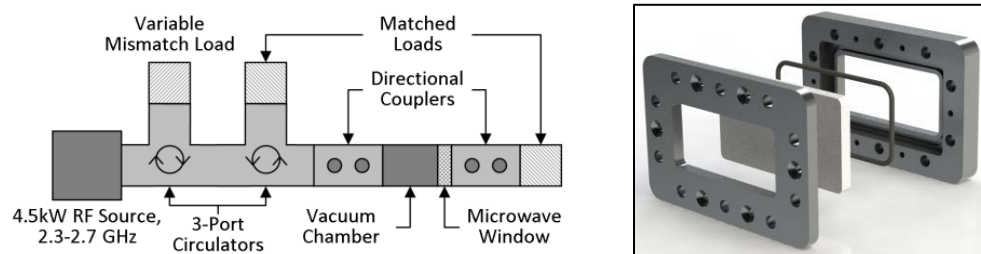


Figure 25: (Left) New experiment configuration. (Right) Basic microwave window design for simplified testing of different conducting networks and materials.

The new experimental setup shown on the left of Fig. 25 preserves the same diagnostics and utilizes the same background gas, but contains several improvements. The first window material to be tested is hexagonal boron nitride (AX05,  $\delta \approx 3$ ), which has a slightly higher secondary yield than Lexan, and is easily machinable. The new microwave source is pulsed ( $\leq 50\mu\text{s}$ ), exhibits fast rise-time ( $< 50\text{ns}$ ), and is frequency-agile (2.3-2.7GHz). Using ferrite circulators, the RF power can be attenuated as low as necessary using a variable mismatch load.

A process has been developed to more easily design and manufacture these microwave windows to simplify the testing of different materials and conducting network patterns. The window shown on the right of Fig. 25 illustrates the basic flange design for mounting different windows. The left side of Fig. 8 shows an example of an embedded conducting network optimization using Maxwell electrostatic simulations to obtain the desired field profile across the window surface. Finally, the right side of Fig. 26 shows how the window iris is optimized using HFSS simulations to match the window impedance to the waveguide impedance.

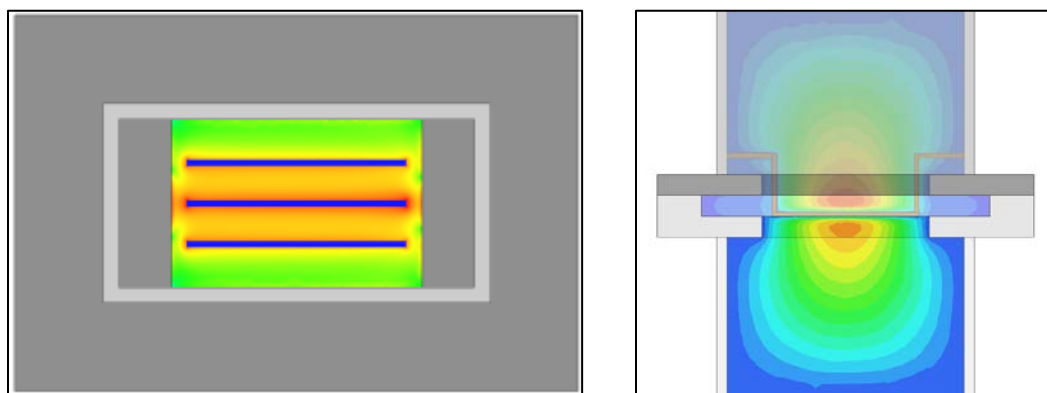


Figure 26: (Left) Example of an electrostatics simulation using Maxwell. (Right) Example of iris optimization to match waveguide impedance using HFSS simulations.

## Summary

To summarize the experimental proof of concept, initial results were encouraging and a -20dB reduction in transmitted power was typically observed. However, operation at higher pressures appears to come at the expense of plasma localization. Window performance degraded over time, and a significant amount of residue was found on the window surface. This is thought to be a thin film formed by plasma interaction with the plastic window.

Ongoing work includes the investigation of RF elimination times, the effect of materials with high secondary electron yields, and targets materials resistant to plasma-induced surface degradation. A framework for testing several window designs is in place, and a new experimental setup has already been constructed.

### 3.1.15 LaB<sub>6</sub>-coated knife-edge field emission

Motivated by the idea of enhancing breakdown with sharp metalized features on or near windows [A-D], we conducted a study of increasing the seed electron emission capability of such metallizations by coating them with a low work function material, specifically LaB<sub>6</sub>. We sputter-deposited LaB<sub>6</sub> films on copper knife-edge field emitters, such as the test structure shown in Fig. 27(a), below. The surprising result, seen in Fig 27(b), was that with 300 nm thick films the emission was reduced rather than increased. However, with very thin (< 10 nm) films the emission *did* increase, as originally expected. Extensive investigation, comparing the results of detailed experiments with quantum mechanical modeling calculations revealed that the interface between a conducting, high work function material and an insulating or semi-conducting low-workfunction material creates a quantum transport barrier for electrons. This barrier reduces the field emission ability of a cathode rather than increases it. When the low work function film is thin enough, then electrons at the interface are able to easily tunnel through this barrier into the film, and the emitted current is higher due to the low workfunction of the deposited film. The computed thin- and thick-film potential profiles showing the barrier at the interface are shown in Fig. 27(c).

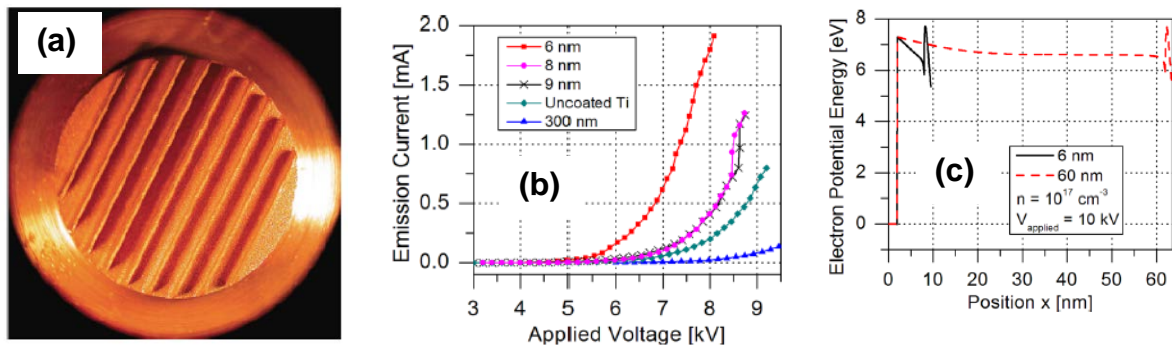


Fig. 27. (a) Photo of uncoated knife edge cathode. (b) I-V characteristics of cathodes with different thicknesses of the LaB<sub>6</sub> coating. Emission is greatly enhanced for thin films and suppressed for thick films. (c) Simulated electron potential energy as a function of position for a thin and thick LaB<sub>6</sub> film at high applied field and low carrier density. The internal barrier is much thinner in the thin LaB<sub>6</sub> film case, resulting in increased tunneling and greater total field emission.

[A] B. Kupczyk, A. Garcia, C.-H. Liu, X. Xiang, N. Behdad, J. Scharer, and J. H. Booske, "Reduced breakdown delay in high power microwave dielectric window discharges," San Francisco, CA, Jun. 2013. [Online]. Available: <http://dx.doi.org/10.1109/PLASMA.2013.6635056>

[B] J. Foster, S. Beeson, M. Thomas, J. Krile, H. Krompholz, and A. Neuber, "Rapid formation of dielectric surface flashover due to pulsed high power microwave excitation," *Dielectrics and Electrical Insulation*, IEEE Transactions on, vol. 18, no. 4, p. 964970, 2011. [Online]. Available: [http://ieeexplore.ieee.org/xpls/abs\\_all.jsp?arnumber=5976082](http://ieeexplore.ieee.org/xpls/abs_all.jsp?arnumber=5976082)

[C] P. Zhang, M. Franzi, Y. Y. Lau, and R. M. Gilgenbach, "Microwave plasma window breakdown theory and experiments," Monterey, CA, 2012.

[D] G. Greening, M. Franzi, P. Zhang, Y. Y. Lau, and R. M. Gilgenbach, "Multipactor-susceptible RF windows as power-tunable microwave limiters," Denver, CO 2013.

### *3.1.16 X-band microwave distributed limiter research results*

After evolving through multiple versions, a mature, versatile, productive experimental system emerged for studying the physics of X-band HPM distributed limiters. Features include:

- ~25 kWp X-band (~9.4 GHz), 800 ns pulse, 43 Hz repetition rate (23 ms between pulses)
- Completely automated operation controlled with MATLAB
- Discharge chamber: stainless steel, 14.6 cm diameter × 15.2 cm long with polycarbonate (PC) windows on each end.
- Precise gas mix control ~ 1 Torr to ~ 300 Torr, gas mixture ratios ranging from 0.1/200 to 1/1, species including Xe, Ar, vs Ne, He
- Time-resolved (from multi-shot aggregated data) OE (optical emission) 3D visual imaging
- Microwave reflection and indicator of power transmission
- Microwave reflection amplitude and phase measurement + 1D equivalent slab model to characterize effective plasma density,  $n_e$ , and (Maxwellian) temperature.  $T_e$
- OES based non-invasive measurements of  $T_{rot}$  ( $T_{gas}$ ) and EEDF
- Design for (not yet implemented) full microwave power transmission diagnostic that also permits single-shot time-resolved spatial imaging of plasma

Figure 28 shows a layout sketch of the entire experimental system and a photograph of the microwave discharge chamber.

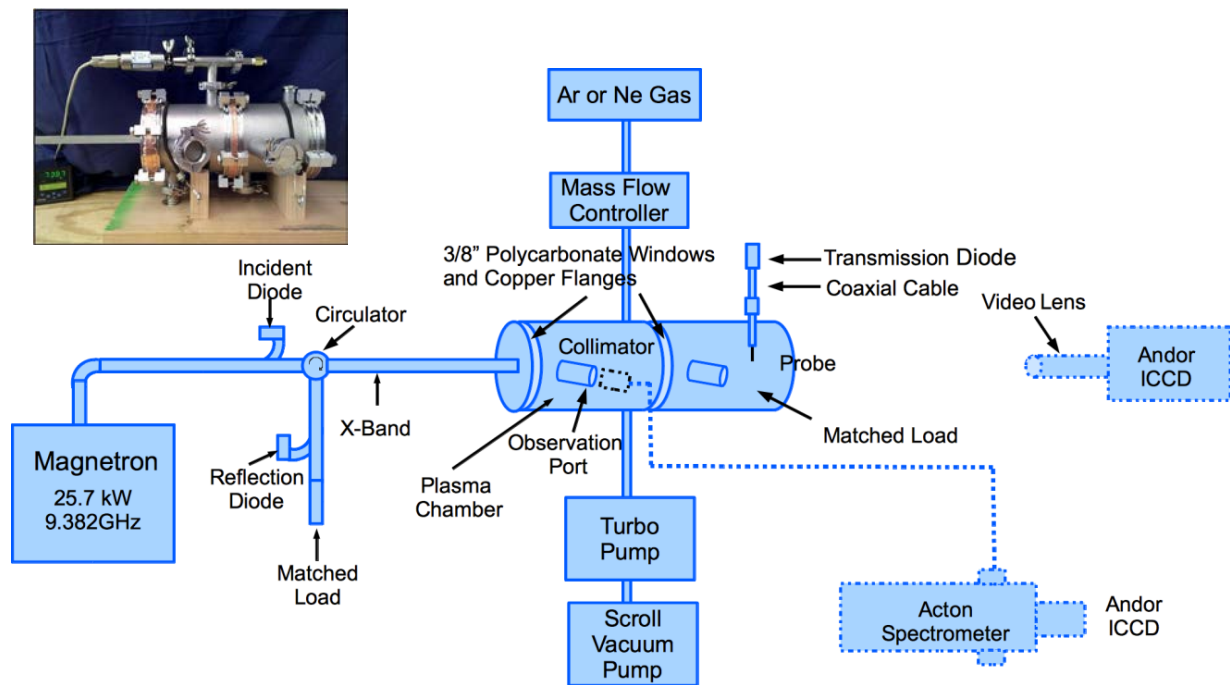


Fig 28. Layout sketch of the X-band distributed limiter system and photo of the microwave discharge chamber.

Breakdown has been repeatedly observed, although only with pulse trains of 3,000-10,000 pulses and not yet with single shot illumination. Here breakdown is “defined” to involve dense and spatially large enough plasma to reflect a detectable fraction ( $> 10\%$ ) of the incident microwave power. Generally, breakdown is first observed between the 2<sup>nd</sup> to the 2000<sup>th</sup> pulse in the pulse train. The likelihood of early (2<sup>nd</sup> pulse) or later (2000<sup>th</sup> pulse) breakdown in the pulse train depends on a number of factors. After the first observation of breakdown in the pulse train, each subsequent pulse exhibits breakdown.

A typical example of the plasma (i.e., its visible light emission’s spatial distribution) is shown in Fig. 29. It forms flush against the inside chamber surface of the PC window, eventually covering an area larger than the X-band aperture, but not the entire window (Figs. 29(b) – (e)). Although not shown in the figure, detectable light emission was observed for approximately 6  $\mu\text{s}$  after the end of the microwave power pulse.

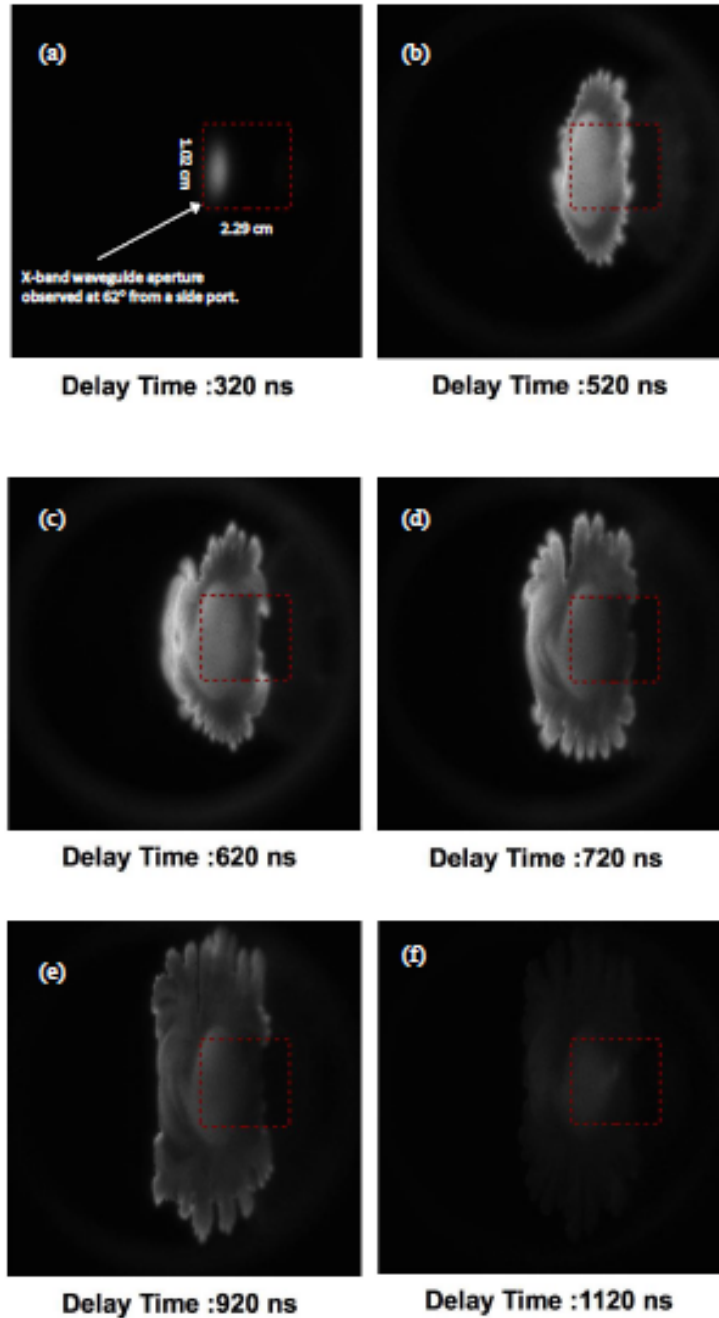


Fig. 29. ICCD images showing time-resolved neon plasma formation and decay process at 100 torr. The exposure time for each picture is 50 ns, and the gain is 200. These pictures are taken from the side port (62 degrees). The red dashed box is the X-band waveguide port.

Microwave power diagnostics are currently the basis for defining the occurrence of “breakdown”, since the application context seeks plasma densities and size sufficient to reflect most of the incident microwave power. Seen below in Fig 30, that happens at  $\sim 150$  ns versus  $\sim 500$ - $600$  ns for the images in Fig. 29. The “breakdown time” varies with gas pressure, gas species, incident microwave power level, etc. Microwave power transmission measurements received by a single centrally located dipole probe at 31.1 cm from the first polycarbonate

window showed a -15 dB received power reduction (97% reflection of the incident power) when the plasma was formed.

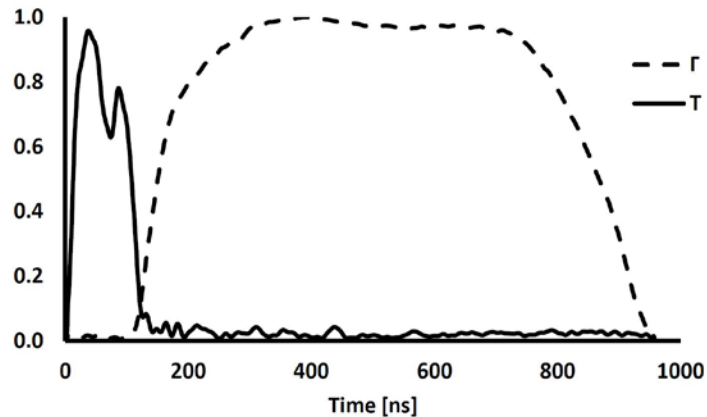


Fig. 29. Illustrative microwave power diagnostics.

By comparing the amplitude and phase of the reflection coefficient measured by microwave diodes and mixers to the six-region, 1-D model, the effective plasma density and electron temperature could be estimated corresponding to an estimated 1 cm maximum plasma thickness. At 100 torr, under a Maxwellian electron energy distribution assumption, the estimated effective plasma density peaked at  $2 \times 10^{12} \text{ cm}^{-3}$ , while the maximum effective electron temperature was 2.5 eV.

An OES study of the plasma was conducted to measure the effective electron temperature in Ne/Ar mixture gas by measuring the 420.1 nm/419.8 nm ( $3p_9-1s_5/3p_5-1s_4$ ) neutral line ratios, allowing the determination of different electron distribution functions between a Maxwellian and a Druyvesteyn. At 100 torr with 2% argon in neon, the line ratio result indicated that the electron energy distribution was not a Maxwellian, but tended somewhat towards a Druyvesteyn distribution that is expected for these highly collisional, unconfined microwave produced plasmas. The above results have been disclosed in several conference presentations and in a journal paper accepted for publication (Journal of Applied Physics, to be published).

Our experiments use magnetron pulse trains with thousands of pulses per pulse train. The pulses are separated by 23 ms (43 Hz). Typically, we do not yet observe breakdown on the first shot in a pulse train. Instead, it takes 2-200 pulses in a pulse train before breakdown is observed, after which all subsequent pulses in the pulse train exhibit nearly identical breakdown characteristics (breakdown time, plasma properties, etc). Figure 30, below, shows data on which pulse in the pulse train exhibits breakdown as a function of number of pulse trains on a given day of experimental runs. For the first pulse train of the day, breakdown (at 150 torr) is not observed until the  $\sim 100^{\text{th}}$  pulse. For the second pulse train, delivered 20 minutes later, breakdown (at 150 torr) is observed to first occur for the  $20^{\text{th}}$  pulse in the pulse train, and similarly for the third pulse train delivered after another 20 minutes. For the fourth pulse train, breakdown first occurs for the 10 pulse in the pulse train. For the fifth and sixth pulse trains (each separated by 20 minutes), breakdown is first observed to occur earlier, for the  $2^{\text{nd}}$  or  $3^{\text{rd}}$  pulse. Thus, there is a memory effect in which breakdown will occur more readily in a pulse-train if it is preceded by

plasma breakdown event(s). By varying the time between pulse-trains, we determined that this memory effect persists for several hours, but disappears after tens of hours (e.g., between two separate days of experiments). Based on lifetimes of excited metastable neutral atoms and the fact that we are constantly purging the gas chamber with new gas supply, this effect has been deduced to result from slow-to-dissipate residual electron charge remaining on the PC window between pulse trains. The delayed breakdown during any one pulse-train is hypothesized to be due to the fact that our experiment’s microwave electric field strength is insufficient to produce enough ionization of a completely neutral (ground state) gas to  $\sim 10^{12} \text{ cm}^{-3}$  plasma densities (required for significant microwave power reflection) in a mere 800 ns. However (we hypothesize), it *is* sufficient to produce smaller fractional ionization and excited metastable atoms, some of which persist on the window (electrons) or in the gas (metastables) for tens of milliseconds (or longer). Each subsequent pulse in a pulse-train has a “headstart” to breakdown over the preceding pulse. Eventually, these “seed electron sources” are sufficiently populated to enable breakdown in all subsequent individual 800 ns pulses. By the time the first pulse with breakdown occurs, we hypothesize the system has established a sustained steady-state population (at the beginning of the pulses) of initial seed electron charge on the window and/or metastables in the gas. Thus, we observe nearly identical breakdown times and time histories of all diagnostic signals between the first pulse to exhibit breakdown and all subsequent pulses in the pulse-train. The results described above indicate that anything that decreases ionization potential (e.g., metastables take less energy to breakdown than ground state atoms) or increases seed electron population (e.g., static electric charge on window surface) has a dramatic effect on the time to breakdown.

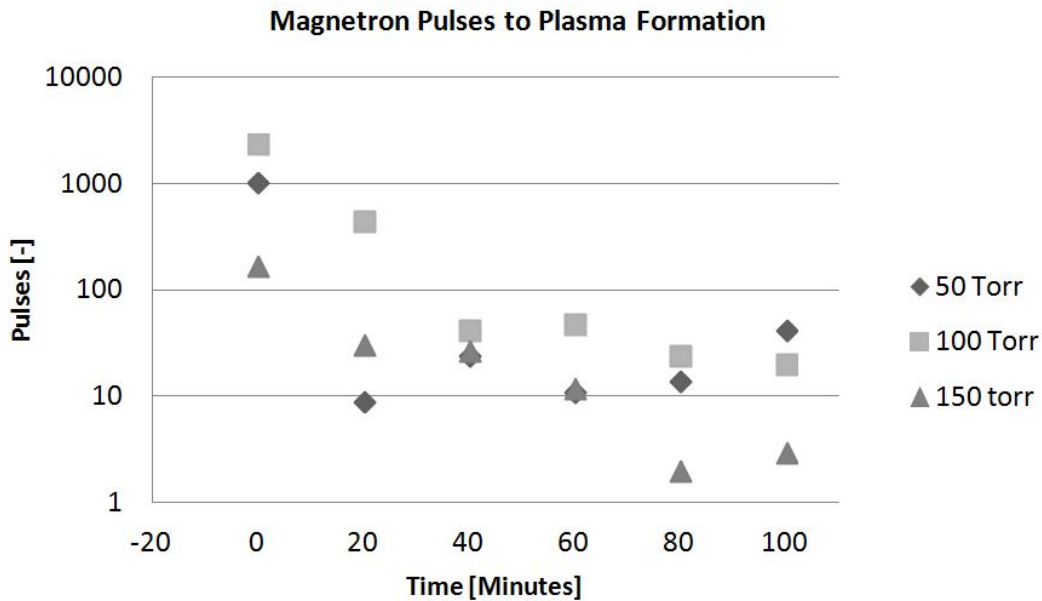


Fig. 30. Required number of pulses in a pulse-train to achieve plasma breakdown for pure neon gas at 50, 100, and 150 torr. Each series was initiated on a separate day with no plasma formation within the plasma chamber for at least 18 hours prior.

### 3.1.17 Penning gas mixture effects on X-band breakdown

The use of Penning gas mixtures to reduce breakdown times or thresholds was proposed in our consortium proposal. The basic idea is to mix a majority population of smaller atoms with lower collision cross-section but higher ionization potentials with a minority population of larger atoms with higher collision cross-sections but lower ionization potentials. The lower collision cross-section of the majority species allows electrons maximum opportunity to gain energy between collisions, even though this gas species is hard to break down due to higher ionization energies. The lower ionization potential of the minority species provides a source of more easily ionized electrons that can act as seed electrons to ionize the atoms of the majority species. We completed a comprehensive study of X-band HPM breakdown with four Penning mixtures (Ar:He, Xe:He, Ar:Ne, Xe:Ne) at 50, 100 and 150 torr and with varying mixture ratios. We identified that fastest breakdown is achieved with a 1:20 ratio of Xe:Ne at 50 torr. The breakdown time of this mix is ~ 62 ns compared with a breakdown time of pure Ne of 136 ns at 50 torr. Results are shown in Fig. 31. This work is being written up for journal publication.

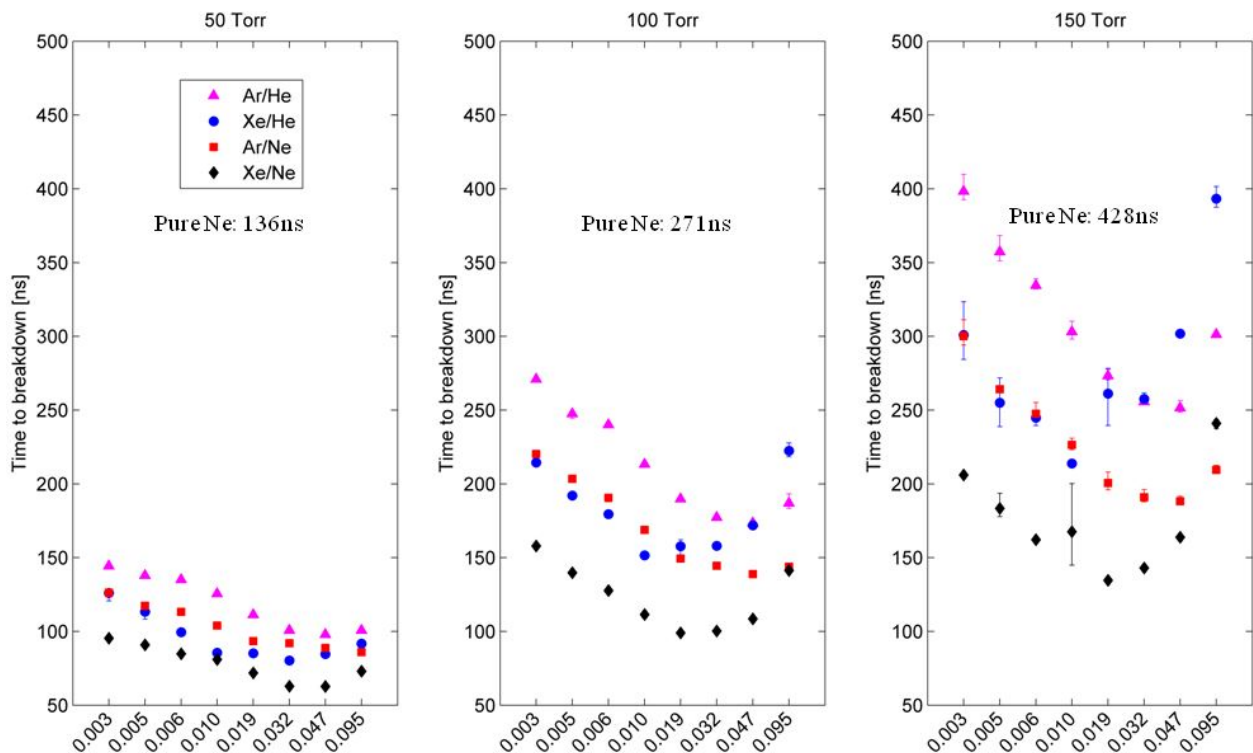


Fig. 31. Data showing that Penning gas mixtures reduce breakdown time compared with pure noble gases such as Ne. Of the mixtures tested, Xe:Ne achieved the fastest breakdown of 62 ns at 50 torr with a Xe:Ne ratio of 1:20. This compares with a breakdown time of 136 ns for pure Ne at 50 torr.

### 3.1.18 Effects of metasurfaces on X-band breakdown

Metamaterials and metasurfaces are heterogenous (typically periodic) structures that function as a homogenous medium, due to fact that unit cell sizes are much smaller than a wavelength. Intentional design and fabrication allows for electromagnetic properties unavailable from natural materials. Experiments with metallic masks layered on the inner surface of our X-band system's transparent PC window demonstrate the potential benefits for distributed HPM limiters. These include

- (1) faster or lower threshold breakdown at designable thresholds, and
- (2) broad area (distributed) protection, prohibiting leakage even when HPM illumination is primarily localized.

An example of a mask is shown in Fig. 32 below. In preliminary experiments, we have observed a reduction in breakdown times with Xe:Ne and Kr:Ne gas mixtures (1:20 ratio at 50 torr) from 60-80 ns without a metasurface to  $\sim 10$ -15 ns when a metasurface mask is used. The main explanation for the enhanced breakdown rate is hypothesized to be the higher local electric fields achieved within the unit cells of the metasurface mask. This research is being written up for journal publication.

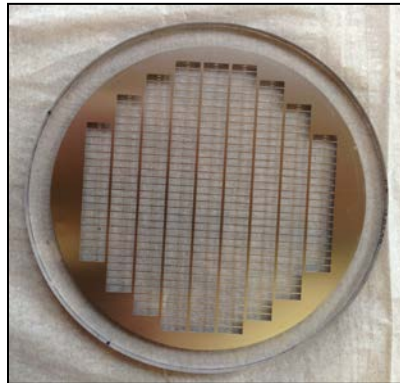


Fig. 32. Photograph of metasurface mask used to reduce breakdown time of Penning gas mixtures from 60-80 ns to 10-15 ns (at 50 torr).

A second, unexpected advantage of using metasurfaces was the observation that plasma breakdown changed from being localized to the center of the window close to the X-band radiation feed aperture to a complete discharge covering the entire window, as shown below in Fig. 33. On the left side, as viewed from the side port, one can see that the plasma is concentrated near the center of the window, where the incident X-band waveguide aperture is located. On the right side, one can see that the breakdown occurs in every unit cell, covering the entire window. This research is being written up for future journal publication. The mechanism for full-window distributed breakdown has been identified as VUV radiation, as revealed in conference papers and in a manuscript that is under review for publication.

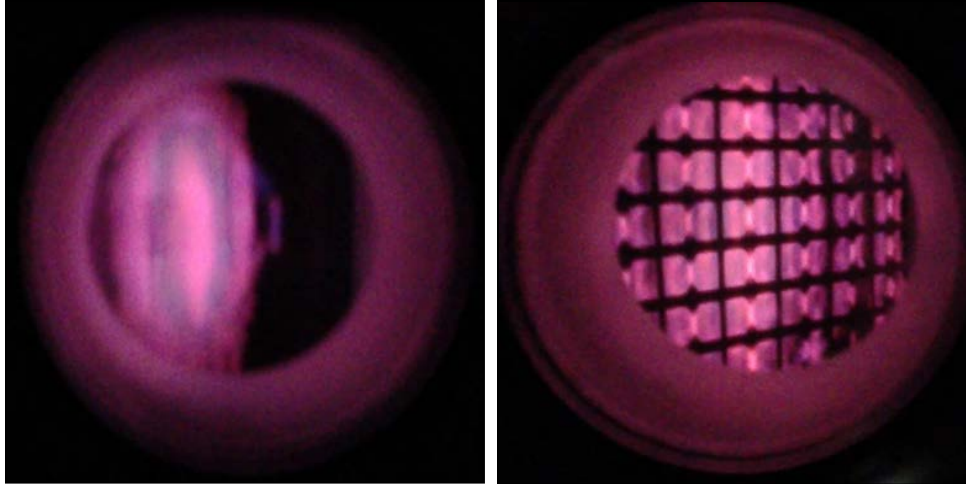


Fig. 33. Left side: localized breakdown concentrated at the center of the window when no metasurface is used (similar to images in Fig. 29). Right side: complete breakdown over full window surface when metasurface mask is used.

## 3.2. Theory and Modeling Achievements

### 3.2.1 High Voltage Dielectric Surface Breakdown

The physics of breakdown of dielectric surfaces under high DC field stress was studied using theoretical models. The development of a number of new models for surface physics of secondary emission and neutral desorption, as well as adding emission distributions has enabled the study of new breakdown physics for angled dielectrics from vacuum to high pressure. A model for surface emission based on the Schächter triple point model was studied, along with fixed current emission and self-consistent field emission models. Two modes of operation were identified for vacuum multipactor: (1) a multipactoring regime in which the surface charges positively due to the secondary emission phenomena, reducing the time of flight of secondary electrons and hence reducing their energy gain, until the impact the surface with an energy sufficient to result in a secondary emission coefficient of unity averaged over the ensemble; and (2), a dark current regime in which the surface charges negatively, and the electrons no longer impact the dielectric but skim the surface until they are collected at the anode side. A particularly interesting result of the study was the transient formation of a multipactor front, which sweeps the surface from cathode to anode at a velocity close to the mean secondary emission velocity. This multipactor front consists of a high density of secondary electrons, and leaves surface charge in its wake. Depending on the parameter space, the surface charge is either positive or negative, resulting in either the multipactoring regime or the dark current regime, as described above. After the front passes, the space charge and currents quickly converge to their steady state values. Holding all other parameters fixed, a dependence of the angle of the dielectric with respect to the electrodes, which affects the vacuum and space charge fields, can be observed with a sharp delineation between the multipactor and dark current modes of operation. The study was

also extended to include the effects of desorption of gas due to surface heating by impacting particles. Due to the slow diffusion of the background gas on breakdown timescales, near surface discharges predominate compared to a uniform background gas. However, in both cases, the surface quickly becomes negatively charged, and multipactor is eliminated.

A new theoretical model for breakdown susceptibility considering time of flight in the early stages of multipactor with known field strength and angles was developed, with good agreement with simulation results. This model allows the mapping of parameter space so that early growth rate of multipactor can be predicted. The model does not presently consider time-dependent surface and space charge, nor the distribution of emission angles and energies of secondaries. Nevertheless, simulation results closely reproduce the predictions, which can include static surface charge. Theoretical understanding of breakdown susceptibility allows engineering methods of breakdown control by understanding field evolution and perturbing the system using external fields to suppress or enhance breakdown as desired.

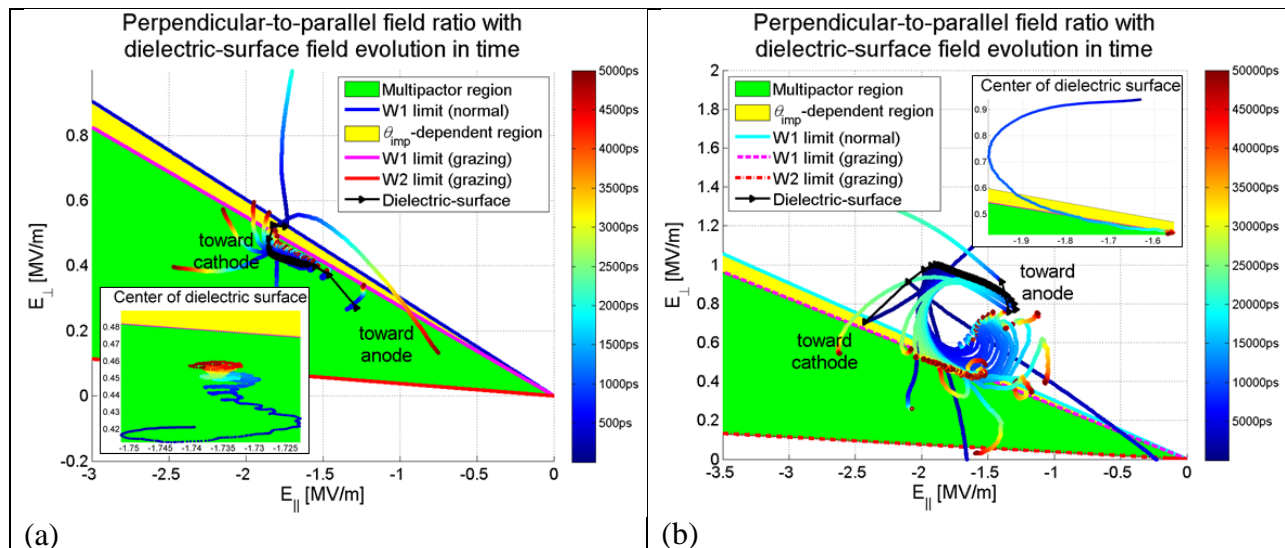


Figure 34. Susceptibility to breakdown for a dielectric surface at (a) 10 deg. and (b) 22.9 deg. from the electrode perpendicular. (a) is an example of a multipactor, while (b) is an example of a dark current. The color traces follow the evolution of the parallel and perpendicular fields in time, with time measured in the color bar. W1 and W2 refer to the lower and upper energy, respectively, for which the secondary emission coefficient exceeds unity.

### 3.2.2 High Pressure Gaseous Breakdown Modeling

The Kinetic Global Model (KGM) was enhanced in a number of ways to better model high pressure gaseous breakdown rapidly. The KGM solves coupled continuity equations for large numbers of species interacting collisionally, for an arbitrary electron distribution function obtained from other models (analytic, particle-in-cell, etc.), along with an electron energy equation which can include electromagnetic wave driving terms. The framework was constructed in Python, enabling user control and programmability of every aspect of operation. The model automatically imports energy dependent cross section data from a number of databases, including LXcat, NIST, CHEMKIN, and others. The imported collision cross sections are convolved with the energy distribution function to obtain reaction rates, which appear as gain and loss terms in the coupled continuity equations. The model includes bidirection rate equilibria, so that inverted populations calculations such as in a laser can be performed.

Efficiency is improved by precompiling code sections once the physics has been determined. The improved model allows flexibility for modeling many high pressure systems in which spatial dependence is not a primary effect. Future work will include analytically determined spatial effects such as sheaths and finite plasma dimensions, by adding terms to the continuity equations to account for net diffusion and wall losses.

### 3.2.3 High Frequency Multipactor on Conducting Surfaces

Multipactor was studied in conducting structures with an added harmonic signal to enhance or suppress the multipactor effect, depending upon phase and amplitude of the added signal. The results demonstrated the complex nature of the spatially and temporally varying phenomena, since suppression in one region often led to enhancement of multipactor in another. However, when the goal is enhancement, a modest enhancement in one area can push a marginal system into a multipactor breakdown event due to the nonlinearity of the breakdown once the averaged secondary emission coefficient exceeds unity for the ensemble. Hence, for a given input signal that might ordinarily fall below breakdown, an additional signal can be used to ensure the combined signals will breakdown, at least locally. The multipactor model was further improved by comparing the Vaughan and Pivi-Furman secondary emission models. The Vaughan model has its roots in the microwave tube community, while the Pivi-Furman model is a recent development in the accelerator community. Although the Pivi-Furman model is much more complicated to construct and use, it has notable physics differences that can be important. In particular, it has a non-zero secondary emission coefficient for low energy impact well below the first cross over energy, where the Vaughan model gives a zero secondary yield. Depending on the electron energy distribution function, this difference can lead to substantial broadening of the multipactor breakdown susceptibility curves, with important implications for the parameter space in which multipactor can occur. The simpler Vaughan model was modified to account for the non-zero low-energy secondary yield, and provided results very similar to the Pivi-Furman model for susceptibility.

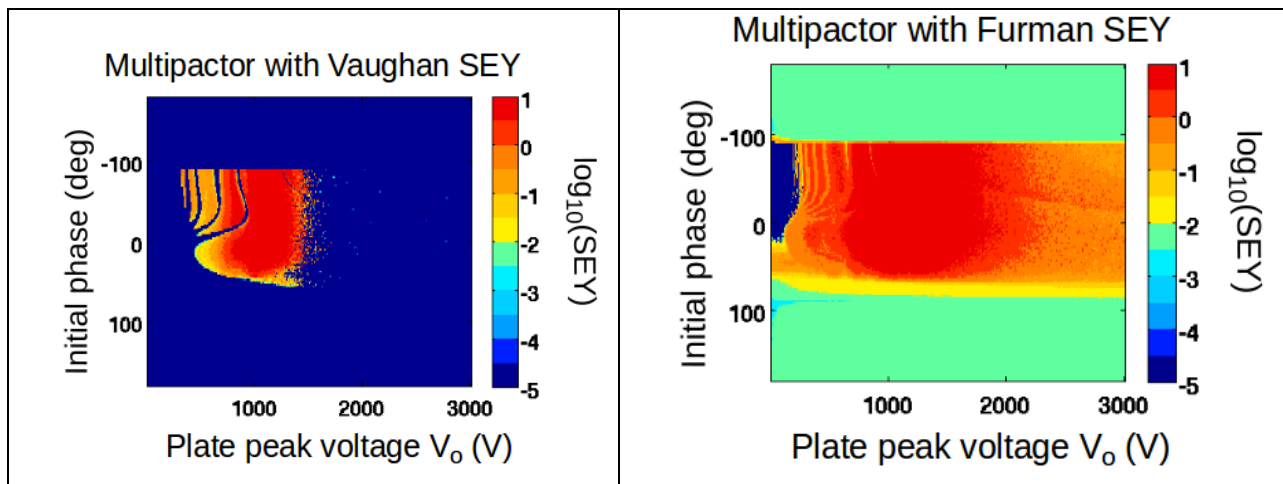


Figure 35. Comparison of multipactor susceptibility for Vaughan and Pivi-Furman secondary emission models.

### 3.2.4 Bipolar Space Charge Limited Flow

The space charge limit has been carefully studied for a wide range of parameters and geometric configurations. However, many forms of low frequency breakdown result in a bipolar flow in which electrons and ions counterstream, with the space charge partially cancelling to allow a higher limiting current. The study of bipolar space charge flow was performed using analytic theory as well as particle-in-cell models, to develop scaling laws from classical to ultra-relativistic regimes. A Python wrapper was developed for the 1D OOPD1 code, in order to automate the search process for the peak current limit while iterating over ion current. The theory agrees very well with the 1D model. In addition, the model was extended to 2D, and the 2D current emission model was improved to properly account for emitted charge weighted to the mesh by the PIC algorithm, so that the field solution would not lead to small oscillations near edges and for non-uniform grids.

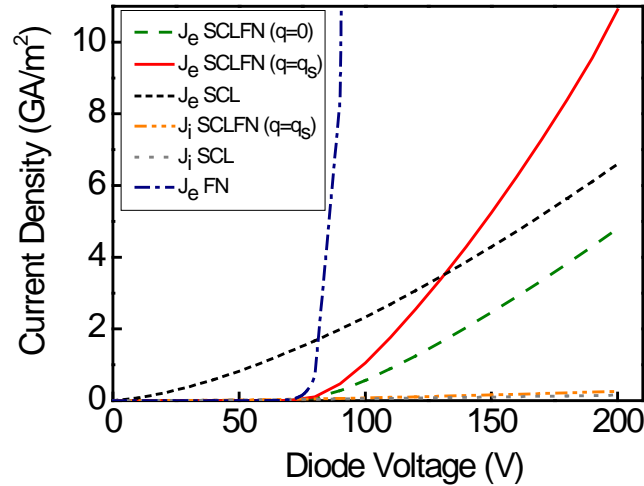


Figure 36. Current density versus voltage in a 1 micron gap.  $q = 0$  indicates the current limit for electron only flow, while  $q = q_s$  denotes the electron current limit in the presence of saturated ion counterflow.

### 3.2.5 Plasma Filaments Formed in High-Power W-Band Breakdown

Previous work on the fundamental theory for plasma filament formation in focused high power W-band beams was extended to consider power levels higher than possible in the original experiments at MIT in which the phenomena was observed. Initial theoretical models indicated that filaments should be spaced apart at the next peak in the standing wave pattern of the fields, at one quarter wavelength ( $\lambda/4$ ). Theory predicts that filament spacing will decrease as power is increased, with the upper limit as minimal breakdown field at the experimentally observed spacing of  $\lambda/4$ , as shown in Fig. 37. As the field strength increases, the breakdown threshold is exceeded before the next peak in the field. This phenomena could lead to the ability to form conductive plasma filament structures with tunable spacing by varying the driving power.

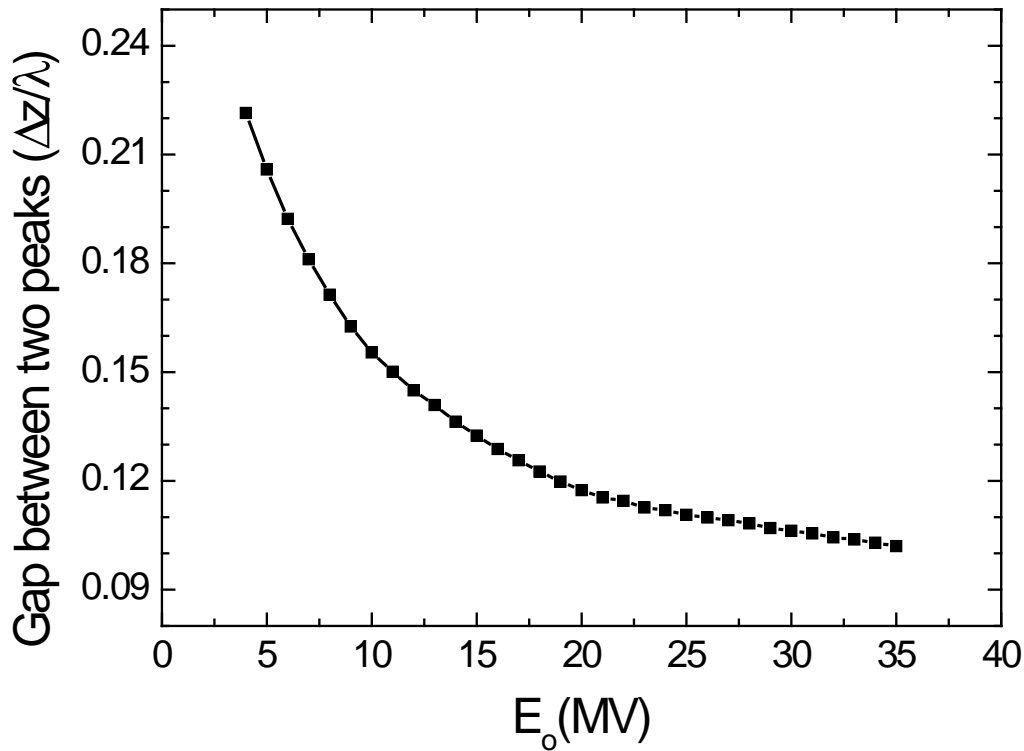


Figure 37. Plasma filament spacing versus field strength for W-band breakdown at 760 Torr.

### 3.2.6 Modeling of the Statistical Nature of Seed Electron Production

A typical simulation of pulsed breakdown or surface flashover in a gaseous environment simply assumes an initial density of free electrons in the gaseous volume. A value of  $\sim 10^3 \text{ cm}^{-3}$  is often quoted as an electron seed value under atmospheric conditions. While the value of a few thousand charged particles in atmospheric air is found throughout the open literature, one discovers, however, little evidence that these charge carriers are indeed free electrons. Rather, one finds that the charge carriers are commonly believed to be comprised of small and large ions. If one also notes that the charge carrier generation rate is only a few tens per cubic centimeter and second, it has to be concluded that there is a very small probability that a free electron is initially available or will be generated in a cubic centimeter sized volume under pulse conditions with a duration of nanoseconds or microseconds. We have gathered strong experimental evidence and developed a model that are consistent with field dependent detachment of electrons from ion clusters in an initially (before pulse application) gaseous volume void of free electrons [E], [F]. The model enables calculating statistical distributions of HPM breakdown, see Fig. 38. A simple generic equation describing the field dependent detachment rate,

$$p(E) = A \cdot E \cdot e^{-B/E} \quad (\text{Eq. 1})$$

was successfully implemented into a 3D Monte Carlo code specifically developed for HPM breakdown at 2.85 GHz. The present model clearly reproduces the experimentally observed statistical variations, which is a dramatic improvement over the previous model and any other previously reported HPM flashover codes. The calculated delay also exhibits an increasing distribution with pressure, correlating well with experimental data, see Fig. 39.

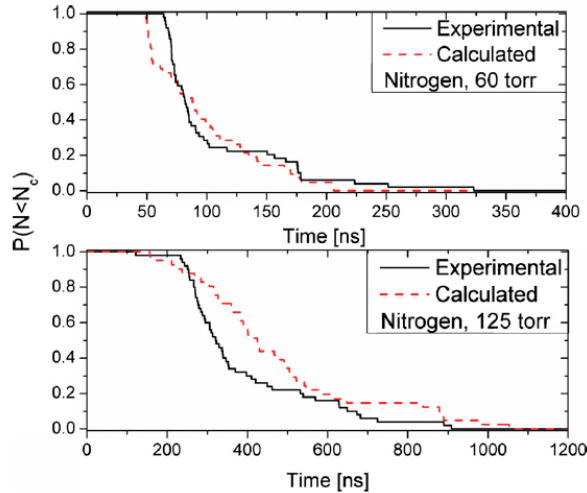


Fig. 38. Measured breakdown statistics. Calculated data are from the developed statistical model based on field detachment of electrons from large ion clusters.

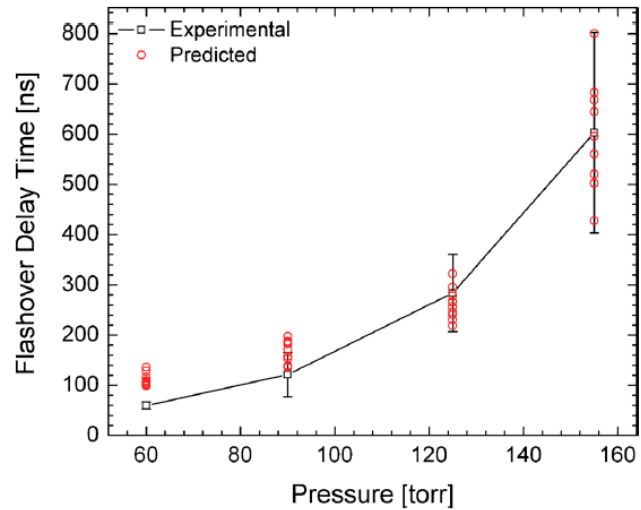


Fig. 39. Comparison of delay times obtained from the of Monte Carlo Code with best fit  $A$  and  $B$  values, cf. Eq. 1,  $1 \times 10^7$  cm/kV s and 75 kV/cm, respectively, with experimentally observed average delay times and standard deviations in air for a 11 kV/cm field amplitude and 50 ns risetime.

Note that simply randomly seeding the volume with free electrons fails to provide the statistics as shown in Fig. 39; all calculated delay times fall on a single line with very little standard deviation at a given pressure. The problem with the free electron seeding approach becomes even more pressing if pulsed unipolar conditions with “slow” voltage ramp up are concerned. During the voltage increase any hypothetically free electrons pulled to the positive electrode before the necessary field for breakdown is established, thus never leading to breakdown. Many models get around this difficulty by simply assuming an infinitely steep voltage step, which of course is not very relevant for many real-world situations.

### 3.2.7 Modeling of unipolar discharge onset in 3D at atmospheric pressure.

In order to expand the statistical seeding model to the unipolar pulse case a 3D PIC/MCC simulation has been developed. It is noted that the development of low-temperature plasmas under pulsed conditions at atmospheric pressure proves to be increasingly difficult to simulate due to the large charged particle numbers encountered. Therefore, many simulations are implemented as reaction/drift/diffusion models with cylindrical (2D) symmetry where the species of interest are tracked as densities. Modern graphics processing units (GPU) have enabled large-scale particle simulations to be performed on standard PC’s. A GPU-accelerated

3D particle-in-cell (PIC)/Monte Carlo Collision (MCC) simulation was developed that utilizes a single NVIDIA GTX Titan (6GB of global memory, 2688 CUDA Cores) to run the code that is developed in a Linux environment in C++ using NVIDIA CUDA. Electron collisions are treated with the null-collision technique that uses a single random number to determine if and what type of collision occurs. An ionization event generates positive and negative space charge that is linearly weighted to the mesh points and coupled to the electric field. Due to the high electric fields near the needle tip, a drift-diffusion approximation for the ions was implemented to allow ion movement rather than assuming static space charge. Photon emission is incorporated where the excited density is determined to radiate by comparing a uniform random number to the solution of the spontaneous emission rate equation. The resulting photons are tracked in a similar manner to electron particles utilizing the null-collision technique and absorption cross sections for photoionization. This differs from other methods of photon implementations such as Helmholtz equation solutions. Initially, the simulation is set to be void of free electron charges. Rather, seed electrons are generated with a semi-empirically derived field-detachment model based on ion-cluster theory as described in [F].

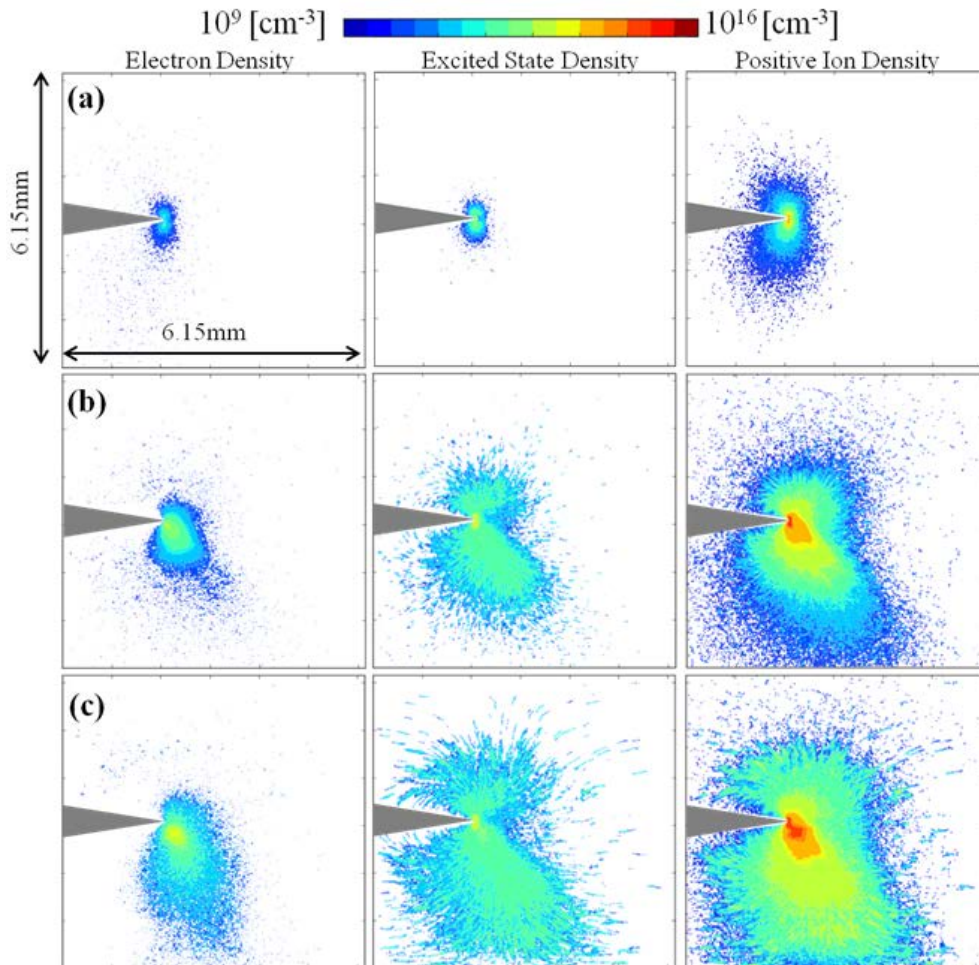


Fig. 40. Spatial distribution profiles of electron, excited state, and ion densities for a positive needle / plane gap in nitrogen at standard temperature and pressure under an applied voltage ramp of 5 kV increased to 9.5 kV over 23.5 ns ( $\sim 200$  V/ns ramp). (a) 2-dimensional cut through needle protrusion tip of density profiles at the time  $t = 22.6$  ns,  $V_{applied} = 9.4$  kV. (b)  $t = 22.9$  ns. (c)  $t = 23.4$  ns. Simulation time of approximately 24 hours on GPU with  $\sim 2 \times 10^6$  particles tracked [G].

Although an axisymmetric background electric field is applied, positive space charge left behind from fast moving electrons moves the high-field region based upon random ionization events causing non-uniform plasma development. Successive simulation runs generated similar results starting with plasma formation near the needle tip; however, each with its own individual shape as one expects from the statistical nature of the electron field detachment and photoionization processes. Future implementations of this code will refine the photo-absorption and emission model to include several photo processes

[E] J. Foster, H. Krompholz, A. Neuber, “Investigation of the Delay Time Distribution of High Power Microwave Surface Flashover,” *Physics of Plasmas* 18, 013502 (2011).

[F] J. Krile and A. Neuber, “Modeling statistical variations in high power microwave breakdown,” *Appl. Phys. Lett.* 98, 211502, (2011).

[G] A. S. Fierro, J. C. Dickens, and A. A. Neuber, “3D Simulation of Low-Temperature Plasma Development Under Pulsed Conditions,” to be published in *IEEE TPS*, 2014.

### 3.2.8 Effects of DC electric field on multipactor

Multipactor discharge is a well-known phenomenon that initiates dielectric window breakdown. To make use of this phenomenon for counter HPM, we introduce a bias DC electric field that is parallel to the dielectric surface. This additional DC electric field is expected to lower the threshold of the RF electric field for multipactor initiation, and therefore, offers a more robust protection of sensitive electronics from HPM attack even at a lower power level. We used analytical calculations and Monte Carlo simulations to derive the condition for the onset of multipactor discharge at various combinations of the bias DC electric field, RF electric field, and background pressures of some noble gases, such as Argon.

It is found that the tangential bias dc electric field on the dielectric surface indeed lowers the magnitude of rf electric field threshold to initiate multipactor. The presence of low pressure gases may lead to a lower multipactor saturation level, however. The combined effects of tangential dc electric field and external gases on multipactor susceptibility are tested in the (UM) proof-of-principle experiment described in the preceding Section 3.1.14.

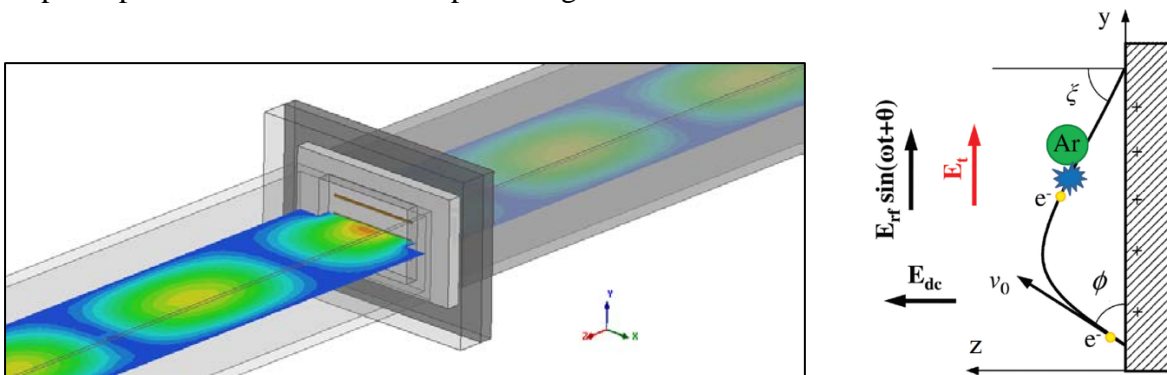


Figure 41: (Left) Example of an HFSS simulation showing  $TE_{10}$  waves incident on a microwave window with an embedded conducting network (Right) Monte Carlo simulation configuration used to determine multipactor susceptibility conditions.

The theoretical basis for the experiment discussed in section 3.1.1 begins by considering the arrangement shown in Fig. 41. The left image shows TE<sub>10</sub> microwaves propagating in a waveguide incident on a microwave window embedded with a horizontally-oriented conducting network designed to manipulate the electric field on the window's surface. Characterization of multipactor susceptibility was accomplished using Monte Carlo simulations of the configuration shown on the right, which shows the microwave window as seen from the side with RF incident from the left.

Simulation results can be seen in Fig. 42. The lower multipactor susceptibility boundary in the left plot demonstrates that increasing the DC bias applied to the conducting network embedded in the RF window effectively pulls the boundary down, which exposes a greater area of the plot to a multipactor-susceptible combination of E<sub>dc</sub> and E<sub>rf</sub>. The plot on the right illustrates a similar effect for different background argon pressures. Most significant is the fact that a configuration that ordinarily would not be expected to be susceptible to multipactor can be made susceptible through a sufficient increase in the tangential electric field E<sub>t</sub> or reduction in background gas pressure. This is the theoretical basis for the power-tunable window in section 3.1.14.

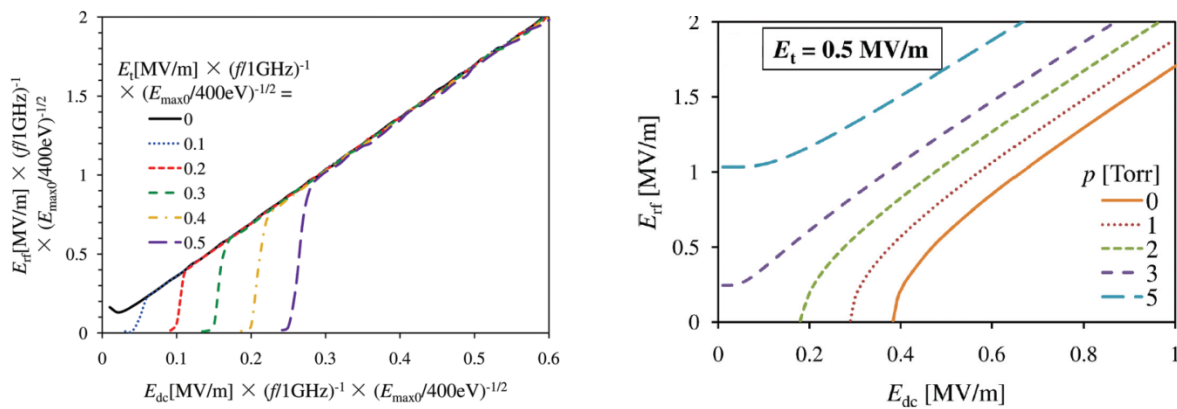


Figure 42: (Left) Lower multipactor susceptibility boundary for variable tangential electric field. (Right) Lower multipactor susceptibility boundary for variable background gas pressure.

Susceptibility was found to be primarily a function of the secondary electron yield  $\delta$  (a material property), the magnitude of the tangential electric field E<sub>t</sub> (provided by the conducting network in a microwave window), and the background gas composition and pressure. Controlling susceptibility to multipactor in an experiment should therefore be possible through the choice of window material, the bias applied to the embedded conducting network, and the background gas composition and pressure.

### 3.2.9 Electrical contacts (rim heating, contrast in heatings in vertical vs horizontal contact)

All junctions involve electrical contact of some sort. RF window is no exception. In fact, Dr. Michael Haworth of AFRL pointed out that RF contacts have always been a most important issue in HPM device performance. Partly for this reason, we launched a massive, systematic study of electrical contacts. We have made vast generalizations on the theory of electrical contact resistance on both bulk and thin film contacts. The effects of dissimilar materials and higher

dimensions are investigated in detail. We found vast difference in the spreading resistance and current crowding behaviors of vertical bulk contact and horizontal thin film contact. However, we also found that the high frequency behavior of vertical bulk contact is very similar to the DC horizontal thin film contact (because the skin depth of the bulk at high frequencies plays the role of a thin film). We found severe current crowding at the rim of the contact electrode, indicating the highest power density dissipation there and therefore the most vulnerable spot for overheating. It would thus not be as helpful simply to increase the contact area to reduce current crowding so as to alleviate the severe Joule heating. Our theoretical study is therefore widely applicable to high power microwave sources, pulsed power systems, field emitters, thin film devices, and interconnects, etc. There was intense interest in this subject at AFOSR a presentation of this work was made there (especially related to the problem of electro-migration due to severe heating at semiconductor contacts). Encouraged by this, we (UM investigators) studied electro-thermo instability as a side project, the result of which is reported in the next subsection.

### 3.2.10 Voltage scale for electro-thermal runaway

We investigated electro-thermal instability (ET) due to the increase in electrical conductivity as temperature increases, which may lead to thermal runaway at fixed voltage. We deduced a voltage scale for ET onset,  $V_s = \sqrt{\kappa/\sigma'_0}$  [in volts], where  $\kappa$  is the thermal conductivity [in W/(m-K)] and  $\sigma'_0$  is the rate of change of the electrical conductivity with respect to temperature [in 1/(ohm-m-K)].  $V_s$  depends only on material properties and is independent of geometry or the operating voltage. It measures the intrinsic tolerance of the material to ET. The calculated  $V_s$  are consistent with the well-known properties of several common materials, such as Si, Ge, C (graphite), and SiC, as summarized in the following table.

Voltage scale for electro-thermal runaway

	$\kappa$ [W/(m-K)] [6-9]	$\sigma'_0$ [1/( $\Omega$ -m-K)] [10-13]	$V_s$ [Volt]
Si	142	0.0012-0.7	14.2-348.9
Ge	58	0.0001-0.05	34-761.6
C (graphite)	127	$1.67 \times 10^{-4}$ - $8.33 \times 10^{-6}$	872.9- 3903.8
SiC	370	$4 \times 10^{-7}$ or negative	$3 \times 10^4$

### 3.2.11 Langmuir-Blodgett law

For breakdown initiation, the maximum current from a local protrusion is of fundamental interest. It is governed by the space charge limited (SCL) condition pertaining to that geometry. For the simple spherical and cylindrical geometry, the SCL current is described by the Langmuir-Blodgett (LB) law, which only gives the SCL current density in numerical forms.

Collaborating with colleagues in Singapore and Iceland, the UM investigators proposed a novel scaling law for the LB solution which depends mainly on the surface electric field on the cathode and the anode-cathode spacing, in a form very different from the LB law and the classical Child-Langmuir scaling. They also obtained a simple empirical formula which is accurate to within 4 percent of the LB law. The model is found to be applicable to space charge limited electron injection into a solid.

## 4. Personnel Supported

### 4.1. MIT

Richard Temkin Associate Director, Plasma Science and Fusion Center  
Michael Shapiro Research Scientist  
William Guss, Research Scientist  
Sudheer Jawla Postdoctoral Associate  
Ivan Mastovsky Engineer  
Paul Thomas Engineer  
Jason Hummelt, Grad Student – Ph. D.  
Elizabeth Kowalski Grad Student – Ph. D.  
Xueying Lu Grad Student Ph. D.  
Brian Munroe Grad Student – Ph. D.  
Emilio Nanni Grad Student – Ph. D.  
Samuel Schaub Grad Student – Ph. D.  
Alexander Soane, Grad Student – Ph. D.  
David Tax Grad Student – Ph. D.  
Haoran Xu Grad Student Ph. D.  
JieXi Zhang Grad Student – Ph. D.  
Jason Bryslawskij Undergrad Student  
Samantha Lewis Undergraduate Student

### 4.2. MSU/UC-Berkeley

#### UC-Berkeley

Manuel Aldan (PhD student)  
Min Ragan-Kelley (PhD student, graduated)  
Jonathan Noland (PhD student, graduated)  
Angelo Wong (undergraduate student researcher)  
S. Taverniers (undergraduate student researcher)  
Dr. Sang Ki Nam (postdoctoral researcher)

#### MSU

Guy Parsey (PhD student)

Scott Rice (PhD student)  
Janez Krek (MS student)  
Dr. Yaman Guclu (postdoctoral researcher)  
Prof. John Verboncoeur

### 4.3. TTU

#### **Faculty/staff**

Dr. Neuber, Andreas  
Dr. Dickens, James  
Dr. Kristiansen, Magne  
Dr. Krompholz, Hermann  
Dr. Frank, Klaus  
Dr. Hatfield, Lynn  
Castro, Dino  
Garcia, Daniel  
Gray, Shannon  
Perez, Joel  
Thornton, Elmer  
Waldrep, Lee

#### **Graduate Students**

Beeson, Sterling  
Clark, Scott E.  
Elsayed, Mohamed  
Fierro, Andrew  
Ford, Patrick  
Foster, Jonathan  
Krile, John  
Laity, George  
Mischke, William  
Ryberg, David  
Stephens, Jacob  
Taylor, Mark  
Thomas, Mark  
Walter, John  
Young, Andrew  
Walls, Michael

### 4.4. UM

#### Students:

P. Zhang, graduated PhD student

Matthew Franzi, PhD student  
Geoffrey Greening, PhD student  
David Simon, PhD student  
Adam Schutt, MS student  
Andrew McKelvey, undergraduate student  
Abe Thurtell, part time technician

Faculty:

Prof. Ronald M. Gilgenbach  
Prof. Y. Y. Lau

Staff:

Dr. Peng Zhang  
Dr. Nicholas Jordan

## 4.5. UW

Graduate Students: Jason Hummelt , Matt Kirley, David Homquist, Carson Cook, Nishant Sule, Xun Xiang, Brian Kupczyk, Paul Carrigan  
Undergraduates: , Kenton Yeates, Abelardo Garcia, Joel Neher

Faculty: John Booske, John Scharer, Nader Behdad

## 5. Publications

### 5.1. Journal publications

1. S. Beeson, J. Dickens, and A. Neuber, "Plasma relaxation mechanics of pulsed high power microwave surface flashover," *Physics of Plasmas* 20(9), 093509 - 093509-9 (2013).
2. G. Laity, A. Fierro, J. Dickens, A. Neuber, and K. Frank, "Simultaneous measurement of nitrogen and hydrogen dissociation from vacuum ultraviolet self-absorption spectroscopy in a developing low temperature plasma at atmospheric pressure," *Appl. Phys. Letters*, 102, 184104, (2013).
3. J. Stephens, S. Beeson, J. Dickens, A. Neuber, "Charged Electret Deposition for the Manipulation of High Power Microwave Flashover Delay Times," *Physics of Plasmas* 19, 112111, 2012.
4. Fierro, G. Laity and A. Neuber, "Optical emission spectroscopy study in the VUV–VIS regimes of a developing low-temperature plasma in nitrogen gas" *J. Phys. D: Appl. Phys.* 45, 11 pages, (2012).

5. P. J. Ford, S. R. Beeson, H. G. Krompholz, and A. A. Neuber, "A finite-difference time-domain simulation of high power microwave generated plasma at atmospheric pressures," *Phys. Plasmas* 19, 073503 (2012).
6. S. Beeson and A. Neuber, "Design and Testing of Multi-Standard Waveguide Couplers," *Rev. Sci. Instrum.* 83, 034702 (2012).
7. J. Foster, H. Krompholz, and A. Neuber, "Statistical analysis of high power microwave breakdown surface flashover delay times in nitrogen with metallic field enhancements," *Phys. Plasmas* 18, 113505, (2011).
8. J. Krile and A. Neuber, "Modeling statistical variations in high power microwave breakdown," *Appl. Phys. Lett.* 98, 211502, (2011).
9. S. Beeson, P. Ford, J. Foster, H. Krompholz, and A. Neuber, "Imaging of Pressure-Dependent High-Power Microwave Surface Flashover," *IEEE Transactions on Plasma Science* 39, 2600-2601, (2011).
10. G. Laity, A. Fierro, L. Hatfield, J. Dickens, and A. Neuber, "Spatially Resolved Vacuum UV Spectral Imaging of Pulsed Atmospheric Flashover," *IEEE Transactions on Plasma Science* 39, 2122-2123, (2011).
11. J. Foster, H. Krompholz, A. Neuber, "Investigation of the Delay Time Distribution of High Power Microwave Surface Flashover," *Physics of Plasmas* 18, 013502 (2011).
12. J. Foster, S. Beeson, H. Krompholz, A. Neuber, "Rapid Formation of Dielectric Surface Flashover due to Pulsed High Power Microwave Excitation," *IEEE Transactions on Dielectrics and Electrical Insulation* 18, pp. 964-970 (2011).
13. G. Laity, A. Neuber, A. Fierro, L. Hatfield, "Phenomenology of Streamer Propagation during Pulsed Dielectric Surface Flashover," *IEEE Transactions on Dielectrics and Electrical Insulation* 18, pp. 946-953, (2011).
14. G. Laity, A. Neuber, G. Rogers, K. Frank, "System for Time Resolved Spectral Studies of Pulsed Atmospheric Discharges in the Visible to VUV Range," *Review of Scientific Instruments*, 81, 083103 (2010).
15. T. Rogers, A. Neuber, G. Laity, K. Frank, J. Dickens, "VUV Emission and Streamer Formation in Pulsed Dielectric Surface Flashover at Atmospheric Pressure," *IEEE Trans. on Plasma Sci.* 38, pp. 2764 – 2770, (2010).
16. J. Krile, L McQuage, G. Edmiston, J. Walter, A. Neuber, "Short Pulse High Power Microwave Surface Flashover at 3 GHz," *IEEE Trans. on Plasma Sci.* 37, pp. 2139-2145 (2009)
17. J. Foster, M. Thomas, A. A. Neuber, "Variation of the statistical and formative time lags of high power microwave surface flashover utilizing a superimposed DC electric field," *J. Appl. Phys.* 106, pp. 063310-063310-4 (2009).
18. Y. Hidaka, E. M. Choi, I. Mastovsky, M. A. Shapiro, J. R. Sirigiri, and R. J. Temkin, G. F. Edmiston, A. A. Neuber, and Y. Oda, "Plasma Structures Observed in Gas Breakdown Using a 1.5-MW, 110-GHz Pulsed Gyrotron", *Phys. Plasmas* 16, 055702 (2009).
19. Y. Y. Lau, D. Chernin, P. Zhang, and R. M. Gilgenbach, "A voltage scale for electro-thermal runaway," *Proc. of IEEE Pulsed Power and Plasma Science* (San Francisco, California, 2013).
20. Y. B. Zhu, P. Zhang, A. Valfells, L. K. Ang, and Y. Y. Lau, "Novel scaling laws for the Langmuir-Blodgett solutions in cylindrical and spherical diodes," *Phys. Rev. Lett.* 110, 265007 (2013).

21. P. Zhang and Y. Y. Lau, "Constriction resistance and current crowding in vertical thin film contact", *IEEE J. Electron Device Soc.* 1, 83 (2013).
22. P. Zhang, D. M. H. Hung, and Y. Y. Lau, "Current flow in a 3-terminal thin film contact with dissimilar materials and general geometric aspect ratios", *J. Phys. D: Appl. Phys.* 46, 065502 (2013).
23. P. Zhang, Y. Y. Lau, and R. S. Timsit, "On the Spreading Resistance of Thin-Film Contacts", *IEEE Trans. Electron Devices*, 59, 1936 (2012).
24. P. Zhang, Y. Y. Lau, and R. M. Gilgenbach, "Thin film contact resistance with dissimilar materials", *J. Appl. Phys.* 109, 124910 (2011).
25. P. Zhang, Y. Y. Lau, M. Franzi and R. M. Gilgenbach, "Multipactor susceptibility on a dielectric with a bias dc electric field and a background gas", *Phys. Plasmas*, 18, 053508 (2011).
26. P. Zhang, Y. Y. Lau, and R. M. Gilgenbach, "Minimization of thin film contact resistance", *Appl. Phys. Lett.* 97, 204103 (2010).
27. P. Zhang, and Y. Y. Lau, "Scaling Laws for Electrical Contact Resistance with Dissimilar Materials", *J. Appl. Phys.* 108, 044914 (2010).
28. G. Greening, et al., "Multipactor-susceptible RF windows as power-tunable microwave limiters," in preparation.
  
29. "Pressure Dependence of Plasma Structure in Microwave Gas Breakdown at 110 GHz," Alan Cook, Michael Shapiro, and Richard Temkin, *Appl. Phys. Lett.*, Vol. 97, 011504, (2010).
30. "Measurements of Electron Avalanche Formation Time in W-Band Microwave Air Breakdown," Alan M. Cook, Jason S. Hummelt, Michael A. Shapiro, and Richard J. Temkin, *Phys. of Plasmas*, Vol. 18, 080707 (2011).
31. "Observation of plasma array dynamics in 110 GHz millimeter-wave air breakdown," A. M. Cook, J. S. Hummelt, M. A. Shapiro, and R. J. Temkin, *Physics of Plasmas*, Vol. 18, Issue 10, 100704 (October, 2011).
32. "Spectroscopic Temperature Measurements of Air Breakdown Plasma Using a 110 GHz Megawatt Gyrotron Beam," J. S. Hummelt, M. A. Shapiro, and R. J. Temkin, *Phys. Plasmas*, Vol. 19, 123509, (2012).
33. "Millimeter wave scattering and diffraction in 110 GHz air breakdown plasma," Alan M. Cook, Jason S. Hummelt, Michael A. Shapiro, and Richard J. Temkin, *Physics of Plasmas* Vol. 20, 043507 (2013).
34. C. S. Meirbachtol, A. D. Greenwood, J. P. Verboncoeur, A. J. Christlieb, and B. Shanker, "Conformal Electromagnetic Particle-in-Cell: A Review and Accuracy Comparison", in preparation (2014).
35. S.-Y. Chen, Y. Güçlü, W.N.G. Hitchon, "Semi-Lagrangian description of electrical breakdown" in preparation (2014).

36. C. Chang, J. Verboncoeur, M. Zhu, M. N. Guo, S. Li, C. H. Chen, X. P. Ouyang, X. C. Bai, J. C. Peng, T. D. Luo, Z. F. Xiong, "Observation of nanosecond development of high power microwave breakdown at a window/air interface", in preparation (2014).
37. S. Rice and J. P. Verboncoeur, "Multipactor Simulation in Coaxial Geometries" submitted IEEE Trans. Plasma Sci. Special Issue on Images in Plasmas 2014.
38. M. C. Lin, P. S. Lu, P. C. Chang, B. Ragan-Kelley, and J. P. Verboncoeur, "A relativistic self-consistent model for studying enhancement of space charge limited field emission due to counter-streaming ions", submitted to Phys. Plasmas (2014).
39. B. Ragan-Kelley, J. P. Verboncoeur, and M.-C. Lin, "Optimizing Physical Parameters in 1-D Particle-in-Cell Simulations with Python", submitted to Comp. Physics Comm. (2014).
40. S. A. Rice and J. P. Verboncoeur, "A Comparison of Multipactor Predictions Using Two Popular Secondary Electron Models", accepted IEEE Trans. Plasma Sci. Special Issue on High Power Microwaves (2014).
41. M. T. P. Aldan and J. P. Verboncoeur, "Simulations of multipactor breakdown in low-pressure background gas for angled dielectrics in DC", IEEE Trans. Diel. Elec. Insul. 20, 1209-1217 (2013).
42. R. H. Jackson, A. C. F. Wu, and J. P. Verboncoeur, "Numerical solution of the cylindrical Poisson equation using the Local Taylor Polynomial technique", J. Comput. Phys. 231, 5421-5442 (2012).
43. C. Chang, J. Verboncoeur, S. Tantawi, and C. Jing, "The effects of magnetic field on single-surface resonant multipactor", J. Applied Phys. 110, 063304 (2011).
44. B. Ragan-Kelley, J. Verboncoeur, and Y. Feng, "Two-dimensional axisymmetric Child--Langmuir scaling law", Phys. Plasmas 16, 103102 (2009).
45. S. K. Nam and J. P. Verboncoeur, "Theory of Filamentary Plasma Array Formation in Microwave Breakdown at Near-Atmospheric Pressure", Phys. Rev. Lett. 103, 055004 (2009).
46. D. Erzen, J. P. Verboncoeur, J. Duhovnik, and N. Jelic, "Simulations of single charged particle motion in external magnetic and electric fields" Euro. Physics J. D54 409-415 (2009).
47. S. K. Nam, C.-H. Lim, and J. P. Verboncoeur, "Dielectric window breakdown in oxygen gas: global model and particle-in-cell approach", Phys. Plasmas 16, 023501 (2009).
48. G. S. Cho, J.-H. Kim, J.-M. Jeong, H. Hwang, D.-J. Jin, J.-H. Koo, E.-H. Choi, J. P. Verboncoeur, and H. S. Uhm, "Plasma Diffusion along a Fine Tube Positive Column", IEEE Trans. Plasma Sci. 37, 438-443 (2009).
49. S. K. Nam and J. P. Verboncoeur, "Global model for high power microwave breakdown at high pressure in air", Comp. Phys. Comm. 180, 628-635 (2009).
50. "Vacuum Electronic High Power Terahertz Sources," John H. Booske, Richard J. Dobbs, Colin D. Joye, Carol L. Kory, George R. Neil, Gun-Sik Park, Jaehun Park, and Richard J. Temkin, **invited review paper**, Inaugural Issue, *IEEE Transactions on Terahertz Science and Technology*, Vol. 1, No. 1, pp. 52-75 (2011).
51. "Effect of Sputtered Lanthanum Hexaboride Film Thickness on Field Emission from Metallic Knife Edge Cathodes," M.P. Kirley, B. Novakovic, N. Sule, M. J. Weber, I. Knezevic, J.H. Booske, *J. Appl. Phys.* Vol 111, No. 6, 063717, 6 pp. (2012).
52. "Investigation of simultaneous breakdown events within a multi-resonant unit cell of high-power metamaterials with discrete nonlinear responses," C.-H. Liu, J. Neher, J.H. Booske, and N. Behdad, *IEEE Trans Plasma Sci* (submitted, 2013).
53. "Reduced Breakdown Delay in High Power Microwave Dielectric Window Discharges

via Penning Gas Mixtures,” B.J. Kupczyk, A. Garcia, X. Xiang, J.E. Scharer, and J.H. Booske, *IEEE Trans. Plasma Sci.* (in preparation, 2013).

54. “Diagnostics of fast formation of distributed plasma discharges using x-band microwaves,” X. Xiang, B.J. Kupczyk, J.H. Booske, and J.E. Scharer, *J Appl Phys* (submitted, 2013).

## 5.2. Conference Papers, Talks, and Abstracts

1. A. Fierro, J. Dickens, and A. Neuber, “Implementation of a 3D PIC/MCC Simulation to Investigate Plasma Initiation in Nitrogen at Atmospheric Pressure,” presented at the 66th Annual Gaseous Electronics Conference, Sept. 30th – Oct. 4th, 2013.
2. J. Stephens, A. Fierro, J. Dickens, and A. Neuber, “A Short Pulse, “High Rep-Rate Microdischarge VUV Source,” presented at the 66th Annual Gaseous Electronics Conference, Sept. 30th – Oct. 4th, 2013.
3. SR Beeson, JC Dickens, AA Neuber, “Post pulse recovery of HPM generated plasma at close to atmospheric pressure,” presented at the IEEE Pulsed Power & Plasma Science Conference, June 16th-21st, 2013.
4. J Stephens, B Loya, J Dickens, A Neuber, “Development and characterization of a pulsed micro hollow cathode discharge array,” presented at the IEEE Pulsed Power & Plasma Science Conference, June 16th-21st, 2013
5. D Ryberg, G Laity, A Fierro, J Dickens, A Neuber, “An experimental system for the measurement of vacuum UV below 115 nm from pulsed plasma in an N<sub>2</sub>/O<sub>2</sub> environment,” presented at the IEEE Pulsed Power & Plasma Science Conference, June 16th-21st, 2013.
6. G Laity, A Fierro, L Hatfield, J Dickens, A Neuber, K Frank, “A passive method for determining plasma dissociation degree using vacuum UV self-absorption spectroscopy,” presented at the IEEE Pulsed Power & Plasma Science Conference, June 16th-21st, 2013
7. S. Beeson, A. Neuber, “Relaxation of High Power Microwave Surface Plasma,” 65th Annual Gaseous Electronics Conference, Vol. 57, Number 8, Oct. 22-16, Austin, TX, 2012.
8. Fierro, G. Laity, A. Neuber, L. Hatfield, “Photon Emission Dynamics during Low-Temperature Plasma Formation,” 65th Annual Gaseous Electronics Conference, Vol. 57, Number 8, Oct. 22-16, Austin, TX, 2012.
9. A. Neuber, J. Stephens, C. Lynn, J. Walter, J. Dickens, M. Kristiansen, “Stand-Alone Pulsed Power Generator for HPM Generation,” Invited Presentation at the 39th IEEE International Conference on Plasma Science, 8-12 July, Edinburgh, UK, 2012.
10. S. Fierro, G. R. Laity, A. A. Neuber, L. L. Hatfield, “Measurements of UV-VUV Radiation Produced from Dielectric Surface Flashover,” presented at the 39th IEEE International Conference on Plasma Science, 8-12 July, Edinburgh, UK, 2012.
11. G. R. Laity, A. S. Fierro, L. L. Hatfield, A. A. Neuber, K. Frank, “Experiments of Vacuum UV Absorption During Low-Temperature Plasma Formation at Atmospheric Pressure,” presented at the 39th IEEE International Conference on Plasma Science, 8-12 July, Edinburgh, UK, 2012.

12. G. Laity, A. Fierro, L. Hatfield, A. Neuber, K. Frank, "Recent Experiments of Vacuum UV Emission and Absorption during Pulsed Atmospheric Breakdown," presented at the EUROEM 2012, 2 – 6 July, Toulouse, France, 2012.
13. S. Beeson, A. Neuber, "Relaxation Times for High Power Microwave Induced Plasma," presented at the EUROEM 2012, 2 – 6 July, Toulouse, France, 2012.
14. S. L. Holt, J.C. Dickens, A. A. Neuber, "Power Electronics for Compact Pulsed Power," 6th Annual RF Munitions And Warhead Workshop, Redstone Arsenal, Huntsville, AL, 2012.
15. S. Beeson, A. Neuber, "Electron Density Evolution of Post-Pulse High Power Microwave Plasma," presented at the 39th IEEE International Conference on Plasma Science, 8-12 July, Edinburgh, UK, 2012.
16. P. Ford, J. Krile, H. Krompholz, A. Neuber, "A Simulation of Breakdown Parameters of High Power Microwave Induced Plasma in Atmospheric Gases," presented at the 2012 International IEEE IPMHV Conference, June 3rd-7th, San Diego, CA (2012)
17. S. Beeson, J. Dickens, A. Neuber, "Evolutions of Plasma Density Generated by High Power Microwaves," presented at the 2012 International IEEE IPMHV Conference, June 3rd-7th, San Diego, CA (2012)
18. G. Laity, A. Fierro, L. Hatfield, A. Neuber, J. Dickens, K. Frank, "Investigation of Vacuum UV Absorption During Low-Temperature Plasma Formation in N<sub>2</sub>/H<sub>2</sub> Mixtures at Atmospheric Pressures," presented at the 2012 International IEEE IPMHV Conference, June 3rd-7th, San Diego, CA (2012)
19. Fierro, G. Laity, A. Neuber, L. Hatfield, "Spatially-resolved Spectral Observations of Pulsed Surface Flashover Plasma in a Nitrogen Environment," presented at the 2012 International IEEE IPMHV Conference, June 3rd-7th, San Diego, CA (2012)
20. P. J. Ford, H. Krompholz, A. Neuber, "A Finite-Difference Time-Domain Simulation of Formative Delay Times of Plasma at High RF Electric Fields in Gases," to be published in Proceedings of the 18th IEEE International Pulsed Power Conference, June 19th – 23rd, Chicago, IL (2011)
21. J. Foster, H. Krompholz, A. Neuber, "Delay Time Distribution of High Power Microwave Surface Flashover," published in Proceedings of the 18th IEEE International Pulsed Power Conference, June 19th – 23rd, Chicago, IL (2011)
22. S. Beeson, J. Foster, J. Dickens, A. Neuber, "Investigation of the Transmission Properties of High Power Microwave Induced Surface Flashover Plasma," published in Proceedings of the 18th IEEE International Pulsed Power Conference, June 19th – 23rd, Chicago, IL (2011)
23. G. Laity, A. Neuber, A. Fierro, J. Dickens, L. Hatfield, "Nanosecond-Scale Spectroscopy of Vacuum Ultraviolet Emission from Pulsed Atmospheric Discharges," to be published in Proceedings of the 18th IEEE International Pulsed Power Conference, June 19th – 23rd, Chicago, IL (2011)
24. Fierro, G. Laity, L. Hatfield, J. Dickens, A. Neuber, "Advanced Imaging of Pulsed Atmospheric Surface Flashover," 18th IEEE International Pulsed Power Conference, June 19th – 23rd, Chicago, IL, (2011).
25. M. Thomas, J. Foster, H. Krompholz, A. Neuber, "High Power Microwave Surface Flashover Seed Electron Production Methods," 2010 IEEE International Power Modulator and High Voltage Conference, May 23 - 27, 2010 in Atlanta, GA.

26. J. Krile, J. Foster, M. Thomas, A. Neuber, "Monte Carlo Simulation of High Power Microwave Surface Flashover under UV Illumination," 2010 IEEE International Power Modulator and High Voltage Conference, May 23 - 27, 2010 in Atlanta, GA.
27. J. Foster, M. Thomas, H. Krompholz, A. Neuber, "Microwave Surface Flashover Using Metallic Initiators," 2010 IEEE International Power Modulator and High Voltage Conference, May 23 - 27, 2010 in Atlanta, GA.
28. K. Frank, J. Dickens, L. Hatfield, M. Kristiansen, G. Laity, A. Neuber, G. Rogers, "First Results of Streamer Formation During Dielectric Surface Flashover at Atmospheric Conditions," DPG Spring Meeting of the Atoms, Molecules, Optics, and Plasmas Section, March 8th - 12th, Hannover, Germany, (2010).
29. G. Laity, A. Neuber, G. Rogers, K. Frank, L. Hatfield, J. Dickens, "Spectral Analysis of Vacuum Ultraviolet Emission from Pulsed Atmospheric Discharges," 37th IEEE International Conference on Plasma Science, June 20th - 24th, Norfolk, VA, (2010).
30. J. T. Krile, L. M. McQuage, J. Walter, J. Dickens, A. A. Neuber, "Short Pulse High Power Microwave Surface Flashover," Proceedings of the 2009 IEEE Pulsed Power Conference (PPC), 129-132, Washington, DC, June 2009.
31. M. Thomas, J. Foster, H. Krompholz, A. Neuber, "Use of Radiation Sources to Provide Seed Electrons in High Power Microwave Surface Flashover," Proceedings of the 2009 IEEE Pulsed Power Conference (PPC), pp. 124-128, Washington, DC, June 2009.
32. J. Foster, M. Thomas, H. Krompholz, A. Neuber, "The Influence of a DC Electric Field on High Power Microwave Window Flashover in Air and N<sub>2</sub> Environments," Proceedings of the 2009 IEEE Pulsed Power Conference (PPC), pp. 480-483, Washington, DC, June 2009.
33. M. A. Franzi, R. M. Gilgenbach, Y. Y. Lau, A. McKelvey, P. Zhang, D. Simon, B. Hoff, "Counter-HPM Window Experiments and Theory", 37th IEEE International Conference on Plasma Science, Norfolk, VA (June 2010).
34. M. Franzi, P. Zhang, R. M. Gilgenbach, and Y. Y. Lau, "Microwave Plasma Window Theory and Experiments", 38th IEEE International Conference on Plasma Science (ICOPS), Chicago, IL (June 2011).
35. M. Franzi, P. Zhang, R. M. Gilgenbach, Y. Y. Lau, and A. McKelvey, "Microwave-Plasma Window Theory and Experiments", 53rd Annual Meeting of the APS Division of Plasma Physics (November 2011, Salt Lake City, Utah).
36. P. Zhang, M. Franzi, Y. Y. Lau, and R. M. Gilgenbach, "Microwave Plasma Window Breakdown Theory and Experiments", 13th International Vacuum Electronics Conference and 9th International Vacuum Electron Sources Conference (April 2012, Monterey, California).
37. G. Greening, M. Franzi, P. Zhang, Y. Y. Lau, A. Schutt, and R. M. Gilgenbach, "Theory and Experimental Characterization of Multipactor RF Window Breakdown", 54th Annual Meeting of the APS Division of Plasma Physics (November 2012, Providence, Rhode Island).
38. G. Greening, M. Franzi, P. Zhang, Y. Y. Lau, A. Schutt, and R. M. Gilgenbach, "Multipactor-Susceptible RF Windows as Power-Tunable Microwave Limiters", 39th IEEE International Conference on Plasma Science (ICOPS), San Francisco, CA (June 2013).

39. G. Greening, M. Franzi, R. M. Gilgenbach, P. Zhang, Y. Y. Lau, and N. M. Jordan, "Multipactor-Susceptible RF Windows as Power-Tunable Microwave Limiters", 55th Annual Meeting of the APS Division of Plasma Physics (November 2013, Denver, Colorado).
40. P. Zhang, Y. Y. Lau, M. R. Gomez, D. M. French, R. M. Gilgenbach, and W. Tang, "PO5.00003: Electrical contact resistance with dissimilar materials", 52nd Annual Meeting of the APS Division of Plasma Physics (November 2010, Chicago, IL, USA).
41. P. Zhang, Y. Y. Lau, and R. M. Gilgenbach, "Thin Film Contact Resistance with Dissimilar Materials – An Exact Formulation", 57th IEEE Holm Conference on Electrical Contacts, Minneapolis, MN USA, No. 56 (September 2011).
42. P. Zhang, Y. Y. Lau, M. R. Gomez, W. Tang, D. M. French, and R. M. Gilgenbach, "Contact Resistance with Dissimilar Materials – Theory and Experiment", 57th IEEE Holm Conference on Electrical Contacts, Minneapolis, MN USA, No. 55 (September 2011).
43. P. Zhang, Y. Y. Lau, R. M. Gilgenbach, "An Exact Formulation of Thin Film Contact Resistance with Dissimilar Materials", 38th IEEE International Conference on Plasma Science (ICOPS), Chicago, IL, USA, IO7B-3 (June 2011).
44. Y. Y. Lau, P. Zhang, W. Tang, M. R. Gomez, D. M. French, J. C. Zier, R. M. Gilgenbach, "UP9.00117: Bulk and Thin Film Contact Resistance with Dissimilar Materials", 53rd Annual Meeting of the APS Division of Plasma Physics (November 2011, Salt Lake City, UT, USA).
45. P. Zhang, Y. Y. Lau, D. Hung, and R. M. Gilgenbach, "JO7.00011: Spreading Resistance on Thin Film Contacts", 54th Annual Meeting of the APS Division of Plasma Physics (November 2012, Providence, Rhode Island, USA).
46. P. Zhang, and Y. Y. Lau, "Recent Development on the Modeling of Electrical Contact", 14th International Vacuum Electronics Conference (May 2013, Paris, France).
47. P. Zhang, and Y. Y. Lau, "Recent development on the modeling of electrical contact", IEEE Pulsed Power & Plasma Science Conference - PPPS 2013 (June 2013, San Francisco, California, USA).
48. Y. Y. Lau, D. P. Chernin, P. Zhang, and R. M. Gilgenbach, "A voltage scale for electro-thermal runaway", IEEE Pulsed Power & Plasma Science Conference - PPPS 2013 (June 2013, San Francisco, California, USA).
49. Y. Y. Lau, D. Chernin, P. Zhang, R. M. Gilgenbach, A. Steiner, "TO5.00005: Voltage scale for electro-thermal runaway", 55th Annual Meeting of the APS Division of Plasma Physics (November 2013, Denver, Colorado, USA).
  
50. Experimental study of highly periodic plasma filament arrays in 110 GHz microwave breakdown Cook, A.; Shapiro, M.; Temkin, R. Plasma Science, 2010 Abstracts IEEE International Conference on ICOPS 2010 (2010)
  
51. Experimental investigation of air breakdown utilizing a 1.5-MW, 110 GHz gyrotron Hummelt, J.S. ; Cook, A.M. ; Shapiro, M.A. ; Temkin, R.J. Plasma Science (ICOPS), 2011 Abstracts IEEE International Conference on (2011)
  
52. Air Breakdown Dynamics with a 1.5-MW, 110 GHz Gyrotron Jason Hummelt, Alan Cook, Michael Shapiro, Rick Temkin, Bulletin of the American Physical Society 64th

Annual Gaseous Electronics Conference Volume 56, Number 15 Monday–Friday, November 14–18, 2011; Salt Lake City, Utah (2011).

53. 1.5 MW, 110 GHz gyrotron breakdown in air Hummelt, J.S.; Cook, A.M.; Shapiro, M.A.; Temkin, R.J. Vacuum Electronics Conference (IVEC), 2012 IEEE Thirteenth International
54. Digital Object Identifier: 10.1109/IVEC., Page(s): 335 – 336 (2012)
55. Experimental characterization of air breakdown plasma utilizing a 1.5MW, 110GHz gyrotron, Schaub, S.C. ; Hummelt, J.S. ; Guss, W.C. ; Temkin, R.J. Plasma Science (ICOPS), 2013 Abstracts IEEE International Conference on (2013).
56. Spatially and Temporally Resolved Electron Density Measurements of Air Breakdown Plasma Utilizing a 1.4 MW, 110 GHz Gyrotron S.C. Schaub, J.S. Hummelt, M.A. Shapiro, R.J. Temkin 55th Annual Meeting of the APS Division of Plasma Physics Volume 58, Number 16 Monday–Friday, November 11–15, 2013; Denver, Colorado (2013).
57. G. Parsey, Y. Guclu, J. Verboncoeur, and A. Christlieb, “Non-Equilibrium Reaction Kinetics of an Atmospheric Pressure Microwave-Driven Plasma Torch: a Kinetic Global Model”, Bull. Am. Phys. Soc. 58:8, MR1-18 (2013).
58. S. Rice and J. Verboncoeur, “A Comparison of Multipactor Predictions Using Two Popular Secondary Electron Models”, IEEE NA-PAC, Pasadena, CA USA (2013).
59. S. Rice and J. Verboncoeur, “Multipactor Suppression Via Secondary Modes In A Coaxial Cavity”, IEEE NA-PAC, Pasadena, CA USA (2013).
60. M. P. Aldan and J. P. Verboncoeur, “Susceptibility of DC Breakdown in Dielectric-Loaded Systems”, 2013 IEEE PPPS, San Francisco, CA USA (2013).
61. H. Bae, J. Y. Lee, H. J. Lee, and J. P. Verboncoeur, “Simulation of Mode Transition and Power Matching in Micro Dielectric Barrier Discharges”, 2013 IEEE PPPS, San Francisco, CA USA (2013).
62. M. P. Aldan and J. P. Verboncoeur, “Characteristics of Gaseous Breakdown in DC for Dielectric-Loaded Systems”, 2013 IEEE PPPS, San Francisco, CA USA (2013).
63. B. Ragan-Kelley and J. Verboncoeur, “Relaxing Assumptions in Field-Limited Emission, and an Iterative Approach to a Scaling Law for Space-Charge Limited Flow in Axisymmetric 2D”, 2013 IEEE PPPS, San Francisco, CA USA (2013).
64. C. Bardel and J. Verboncoeur, “Increasing Efficiency of Monte Carlo Particle-Fluid Collision Calculations on GPU”, 2013 IEEE PPPS, San Francisco, CA USA (2013).
65. G. Parsey, Y. Güçlü, J. Verboncoeur, and A. Christlieb, “Non-Equilibrium Kinetics of a Microwave-Assisted Jet Flame: Global Model and Comparison with Experiment”, 2013 IEEE PPPS, San Francisco, CA USA (2013).
66. S. Rice and J. Verboncoeur, “Multipactor Suppression in Resonant Cavities via Higher-Order Modes”, 2013 IEEE PPPS, San Francisco, CA USA (2013).
67. N. Jelic, L. Kos, J. Krek, J. Kovacic, T. Gyergyek, A. J. Christlieb, J. P. Verboncoeur, “Ionization front in a gas-filled diode during electrical breakdown”, 49<sup>th</sup> International Conference on Microelectronics, Devices, and Materials, Kranjska Gora, Slovenia (2013).

68. B. Ragan-Kelley, J. Verboncoeur, and M.-C. Lin, "Programmable physical parameter optimization for particle plasma simulations", *Bull. Am. Phys. Soc.* 57:12, UP8.00008 (2012).
69. J. P. Verboncoeur, G. Parsey, Y. Guclu, and A. J. Christlieb, "Python framework for kinetic modeling of electronically excited reaction pathways", *Bull. Am. Phys. Soc.* 57:12, TP8.00088 (2012).
70. M. Aldan and J. P. Verboncoeur, "Simulation of High-Voltage DC Breakdown for Angled Dielectric Insulators including Space-Charge and Gas-Collision Effects", *Bull. Am. Phys. Soc.* 57:12, BO6.00004 (2012).
71. R. H. Jackson and J. P. Verboncoeur, "Analytic sources using polynomial shaped particles in the LTP method", 39th IEEE ICOPS, Edinburgh, Scotland (2012).
72. M. P. Aldan and J. P. Verboncoeur, "Simulation of high-voltage DC breakdown for angled dielectric insulators including space-charge and gas-collision effects", 39th IEEE ICOPS, Edinburgh, Scotland (2012).
73. M. C. Lin, P. S. Lu, P. C. Chang, and J. P. Verboncoeur, "Influence of ion effects on a space charge limited field emission flow: from non-relativistic to ultra-relativistic regimes", 39th IEEE ICOPS, Edinburgh, Scotland (2012).
74. M. P. Aldan and J. P. Verboncoeur, "Numerical Particle Heating And Diffusion Correlated To Interpolation-induced Divergence In A Static Magnetic Field For PIC Simulations", 39th IEEE ICOPS, Edinburgh, Scotland (2012).
75. M. P. Aldan and J. P. Verboncoeur, "Simulation of high-voltage DC breakdown for angled dielectric insulators including space-charge and gas-collision effects", IEEE International Power Modulator and High Voltage Conference, San Diego, CA USA (2012).
76. R. H. Jackson and J. P. Verboncoeur, "Analytic sources using polynomial shaped particles in the LTP method", IEEE International Power Modulator and High Voltage Conference, San Diego, CA USA (2012).
77. M. C. Lin, P. C. Chang, P. S. Lu, and J. P. Verboncoeur, "Influence of Ion Effects on a Space-Charge Limited Field-Emission Flow: From NonRelativistic to Ultra-Relativistic Regimes", IEEE Vacuum Electronics Conference, Monterey, CA (2012).
78. M. C. Lin, P. S. Lu and J. P. Verboncoeur, "An improved self-consistent fitting model for characterizing field emitters ", IEEE Vacuum Electronics Conf., Bangalore, India (2011).
79. B. Ragan-Kelley and J. Verboncoeur, "Interactive, Extensible PIC Simulations with a Python Interface ", *Bull. Am. Phys. Soc.* 56, NP9.00030 (2011).
80. M. Aldan and J. Verboncoeur, "Modeling High-Voltage Breakdown for Angled Dielectric Insulators ", *Bull. Am. Phys. Soc.* 56, JW3.00007 (2011).
81. M. C. Lin, P. C. Chang, P. S. Lu, J. P. Verboncoeur, "Influence of ion effects on a space charge limited field emission flow: from non-relativistic to ultra-relativistic regimes ", *Bull. Am. Phys. Soc.* 56, YP9.00042 (2011).
82. M. C. Lin and J. P. Verboncoeur, "An Improved Self-consistent Fitting Model for Characterizing Field Emitters", *Bull. Am. Phys. Soc.* 55, UP9.00145 (2010).
83. M. Aldan, J. Verboncoeur, Y. Y. Lau, and J. Booske, "Modeling High-Voltage Breakdown for Single- and Multi-stack Dielectric Insulators", *Bull. Am. Phys. Soc.* 55, TP9.00037 (2010).

84. M. P. Aldan, J. P. Verboncoeur, and R. L. Ives, "Simulation of high-voltage dc breakdown for angled dielectric insulator including space-charge effects" 37th IEEE ICOPS, Norfolk, VA USA (2010).
85. J. P. Verboncoeur, A. C. Wu, R. H. Jackson, and T. Bui, "Improved space charge modeling in cylindrical coordinates", 37th IEEE ICOPS, Norfolk, VA USA (2010).
86. M. P. Aldan, J. P. Verboncoeur, and R. L. Ives, "Simulation of high-voltage DC breakdown for angled dielectric insulator including space-charge effects", IEEE Power Mod. High Volt. Conf., Atlanta, GA USA (2010).
87. J. P. Verboncoeur, A. C. Wu, R. H. Jackson, and T. Bui, "Improved space charge modeling in cylindrical coordinates", IEEE Power Mod. High Volt. Conf., Atlanta, GA USA (2010).
88. M. P. Aldan, J. P. Verboncoeur, and R. L. Ives, "Simulation of high-voltage DC breakdown for angled dielectric insulator including space-charge effects", International Vacuum Electronics Conference, Monterey, CA USA (2010).
89. R. H. Jackson, T. Bui, A. C. Wu, and J. P. Verboncoeur, "Improved space charge modeling in cylindrical coordinates", International Vacuum Electronics Conference, Monterey, CA USA (2010)
90. J. P. Verboncoeur, M. Aldan, and S. Taverniers, "2D particle-in-cell modeling of dielectric insulator breakdown", Bull. Am. Phys. Soc. 54, PP8.00105 (2009).
91. M. C. Lin, P. C. Chang, and J. P. Verboncoeur, "Influence of Ion Effects on a Space Charge Limited Field Emission Flow: From Classical to Ultrarelativistic Regimes", Bull. Am. Phys. Soc. 54, Q14.5 (2009).
92. J. P. Verboncoeur, "Computer Experimentation: Particle-in-Cell Simulation of Collisional Plasmas", 19th Int. Symp. Plasma Chem., Bochum, Germany (2009) invited.
93. J. P. Verboncoeur and S. K. Nam, "An Enhanced Global Model for High Pressure Microwave-Driven Gaseous Breakdown", 19th Int. Symp. Plasma Chem., Bochum, Germany (2009).
94. M.A. Lieberman, E. Kawamura<sup>1</sup>, A.J. Lichtenberg, and J.P. Verboncoeur, "Double layer formation in a two-region electronegative plasma", 19th Int. Symp. Plasma Chem., Bochum, Germany (2009) invited.
95. S. Taverniers, C.-H. Lim, and J. P. Verboncoeur, "2d particle-in-cell modeling of dielectric insulator breakdown", 36th IEEE ICOPS, San Diego, CA (2009).
96. S. K. Nam and J. P. Verboncoeur, "Theory of filamentary plasma array formation in microwave breakdown at near atmospheric pressure", 36th IEEE ICOPS, San Diego, CA (2009).
97. M.P. Aldan and J.P. Verboncoeur, "Particle heating in magnetized plasmas with interpolation-induced divergence", 36th IEEE ICOPS, San Diego, CA (2009).
98. M.-C. Lin, P. C. Chang, and J. P. Verboncoeur, "Influence of ion effects on a space charge limited field emission flow: from nonrelativistic classical to ultrarelativistic regimes", 36th IEEE ICOPS, San Diego, CA (2009).
99. Nishant Sule, Matt Kirley, Bozidar Novakovic, John Scharer, Irena Knezevic and John H. Booske "Examination of field emission from copper knife edge cathodes with low-work function coatings", 11<sup>th</sup> IEEE Int'l Vacuum Electronics Conference (Monterey, CA, 2010).

100. David Holmquist, Matt Kirley, Carson Cook, John Scharer and John Booske “Distributed Discharge Limiter Studies for X-band High Power Microwaves”, 11<sup>th</sup> IEEE Int’l Vacuum Electronics Conference (Monterey, CA, 2010).
101. N. Sule, M. Kirley, B. Novakovic, J. Scharer, I. Knezevic, and J.H. Booske, “Field emission from low work function cathode coatings,” Intl. Conf. Plasma Science, Norfolk, VA, 2010.
102. D. Homlquist, M. Kirley, C. Cook, J. Scharer, J. Booske, “Breakdown limiter studies for high power X-band Microwaves,” Intl. Conf. Plasma Science, Norfolk, VA, 2010.
103. Nishant Sule, Matt Kirley, Bozidar Novakovic, John Scharer, Irena Knezevic and John H. Booske “Examination of field emission from copper knife edge cathodes with low-work function coatings”, 11<sup>th</sup> IEEE Int’l Vacuum Electronics Conference (Monterey, CA, 2010).
104. David Holmquist, Matt Kirley, Carson Cook, John Scharer and John Booske “Distributed Discharge Limiter Studies for X-band High Power Microwaves”, 11<sup>th</sup> IEEE Int’l Vacuum Electronics Conference (Monterey, CA, 2010).
105. N. Sule, M. Kirley, B. Novakovic, J. Scharer, I. Knezevic, and J.H. Booske, “Field emission from low work function cathode coatings,” Intl. Conf. Plasma Science, Norfolk, VA, 2010.
106. D. Homlquist, M. Kirley, C. Cook, J. Scharer, J. Booske, “Breakdown limiter studies for high power X-band Microwaves,” Intl. Conf. Plasma Science, Norfolk, VA, 2010.
107. John Scharer, John Booske, David Holmquist and Brian Kupczyk, “Distributed Discharge Limiter Studies for High Power X-Band Microwaves,” Air Force Office of Scientific Research (AFOSR) Open House & Kick-Off Meeting: Counter High Power Microwaves (July 2010, Albuquerque, NM, USA).
108. David Holmquist, Brian Kupczyk, Marcus Weber, John Scharer, Jason Hummelt, Matt Kirley and John Booske, “Distributed Discharge Limiter Studies for X-band High Power Microwaves,” Air Force Office of Scientific Research (AFOSR) Open House & Kick-Off Meeting: Counter High Power Microwaves (July 2010, Albuquerque, NM, USA).
109. J. Scharer, J. Booske, R. Gilgenbach, R. Temkin, A. Neuber, J. Verboncour, “High Frequency Gaseous Breakdown Research on Distributed Plasma Discharges,” High Frequency Breakdown Workshop, Gaseous Electronics Conference, Paris, France, October 4, 2010.
110. David Holmquist, John Scharer, Biran Kupczyk and John Booske, “High Frequency Gaseous Breakdown Research on Distributed Plasma Discharges,” American Physical Society Division of Plasma Physics Annual Meeting, Chicago, IL, Nov. 8-12, 2010.

111. M. Kirley, B. Navokovic, M. Weber, N. Sule, J. Scharer, I. Knezevic, and J.H. Booske, "Examination of Field Emission from Lanthanum Hexaboride Coated Knife Edge Cathodes," 12<sup>th</sup> IEEE International Vacuum Electronics Conference, Bangalore, India, February 22-24, 2011.
112. D. Holmquist, B. Kupczyk, X. Xiang, J. Booske and J. Scharer, "Rapid Formation of Distributed Plasma Discharges using X-Band Microwaves," 38th IEEE International Conference on Plasma Science and 24th Symposium on Fusion Engineering, Chicago, IL, June 26-30, 2011.
113. X. Xiang, B. Kupczyk, J. Booske and J. Scharer, "Rapid Formation of Distributed Plasma Discharges using X-Band Microwaves," 53rd Annual Meeting of the APS Division of Plasma Physics, Salt Lake City, Ut, November 14-18, 2011.
114. B. Kupczyk, X. Xiang, M. Kirley, J. Scharer and J. Booske, "Evaluation of Breakdown Delay in High Power Microwave Dielectric Barrier Discharges," 53rd Annual Meeting of the APS Division of Plasma Physics, Salt Lake City, Ut, November 14-18, 2011.
115. M. Kirley, B. Navokovic, M. Weber, N. Sule, J. Scharer, I. Knezevic, and J.H. Booske, "Examination of Field Emission from Lanthanum Hexaboride Coated Knife Edge Cathodes," 12<sup>th</sup> IEEE International Vacuum Electronics Conference, Bangalore, India, February 22-24, 2011.
116. D. Holmquist, B. Kupczyk, X. Xiang, J. Booske and J. Scharer, "Rapid Formation of Distributed Plasma Discharges using X-Band Microwaves," 38th IEEE International Conference on Plasma Science and 24th Symposium on Fusion Engineering, Chicago, IL, June 26-30, 2011
117. B. Kupczyk, X. Xiang, J. Scharer, J. Booske, "Characterization of breakdown delay and memory effects in high power microwave dielectric window discharges," IEEE International Conference on Plasma Science, Edinburgh, UK (July 8-12, 2012).
118. X. Xiang, B. Kupczyk, J. Booske, J. Scharer, "Rapid formation of distributed plasma discharges using X-band microwaves," 54th Annual Meeting of the APS Division of Plasma Physics, Providence, RI, (October 29-November 2, 2012).
119. B. Kupczyk, X. Xiang, J. Scharer, and J. Booske, "Reduced breakdown delay via memory and penning effects in high power microwave dielectric window discharges," 54th Annual Meeting of the APS Division of Plasma Physics, Providence, RI, (October 29-November 2, 2012).
120. John. Booske, Susan Hagness, Irena Knezevic, Dane Morgan, John Scharer, Nils Carlsson, David Holmgren, Ryan Jacobs, Sarah Katz, Matt Kirley, Brian Kupczyk, Marcus Weber, Xun Xiang, Ben Yang, "AFOSR-funded research at University of Wisconsin-Madison," AFOSR Workshop, San Antonio, Texas, January 16, 2012.

121. X.Xiang, B. Kupczyk, J. Booske, J. Scharer, "Rapid Formation of Distributed Plasma Discharges Using X-Band Microwaves," IEEE Pulsed Power and Plasma Science (PPPS) Conference, (San Francisco, CA, June 16-21, 2013).
122. B. Kupczyk, C.H. Liu, X. Xiang, J. Scharer, N. Behdad, J. Booske, "Reduced Breakdown Delay in High Power Microwave Dielectric Window Discharges," IEEE Pulsed Power and Plasma Science (PPPS) Conference, (San Francisco, CA, June 16-21, 2013).
123. J. Scharer, X. Xiang, B. Kupczyk, J. Booske, "Rapid X-Band Microwave Breakdown in Ne," IEEE Pulsed Power and Plasma Science (PPPS) Conference, (San Francisco, CA, June 16-21, 2013).
124. J. Booske, B. Kupczyk, A. Garcia, C.-H. Liu, X. Xiang, N. Behdad, J. Scharer, "Reduced Breakdown Delay in High Power Microwave Dielectric Window Discharges via Penning-Like Mixtures and Patterned Metallizations," 55<sup>th</sup> Annual Meeting of the American Physical Society Division of Plasma Physics (Denver, CO, November 11-15, 2013).
125. X. Xiang, B. Kupczyk, J. Booske, J. Scharer, "Rapid Formation of Distributed Plasma Discharges using X-Band Microwaves," 55<sup>th</sup> Annual Meeting of the American Physical Society Division of Plasma Physics (Denver, CO, November 11-15, 2013).
126. C.-H. Liu, J. Neher, J. Booske, N. Behdad, "Investigating the Physics of Microwave Induced Breakdown in Metamaterials with Multi-Resonant Constituting Unit Cells," 55<sup>th</sup> Annual Meeting of the American Physical Society Division of Plasma Physics (Denver, CO, November 11-15, 2013).
127. J. Scharer, X. Xiang, B. Kupczyk, J. Booske, "Rapid X-Band Microwave Breakdown in Ne/Ar," 55<sup>th</sup> Annual Meeting of the American Physical Society Division of Plasma Physics (Denver, CO, November 11-15, 2013).
128. Chien-Hao Liu, John H. Booske, and Nader Behdad, Investigating Failure Mechanisms in High-Power Microwave Frequency Selective Surfaces , 2014 IEEE Antennas and Propagation Society International Symposium
129. C.-H. Liu, J. Neher, J.H. Booske, N. Behdad, Investigating the Physics of Simultaneous Breakdown Events in Metamaterials with Multi-Resonant Unit Cells, 15<sup>th</sup> IEEE International Vacuum Electronics Conference, April 22-24, 2014, Monterey, CA.

## 6. Honors and Awards

## 6.1. Co-PI's (during this grant)

Dr. A. Neuber: Fellow of the Institute of Electrical and Electronics Engineers, 2012; Distinguished AT&T Professor (2011); IEEE William Dunbar Award for "Continuing Contributions to High Voltage Research, Technology, and Engineering Education", 2010

Dr. Richard Temkin: IEEE Plasma Science and Applications Award (2013); Exceptional Service Award, Intl. Soc. Infrared, Millimeter, and Terahertz Waves (2011).

Dr. John Booske: University of Michigan, College of Engineering Alumni Merit Award; Nuclear Engineering and Radiological Sciences Department recipient (2012); Elected Fellow of the American Physical Society (2011); Re-selected for second term to receive the Duane H. and Dorothy M. Bluemke Professor endowed chair (2010); Selected as a 2009-10 Fellow in the Committee on Institutional Cooperation (CIC) Academic Leadership Program (ALP). The CIC is a consortium of 12 research universities, including the 11 members of the Big Ten Conference and the University of Chicago.

## 6.2 Other personnel

1. Jacob Stephens, TTU, received the 2013 Art Guenther outstanding graduate student award sponsored NPSS IEEE.
2. George Laity, TTU, won the best student paper competition at the IEEE Pulsed Power & Plasma Science Conference in San Francisco, California, June 16-21, 2013
3. Andrew Fierro, TTU, received the 2013 Institute of Electrical and Electronic Engineers Dielectrics and Electrical Insulation Society (IEEE-DEIS) fellowship aimed at students pursuing their Ph.D. degree.
4. Sterling Beeson, TTU, received the 2013 IEEE Nuclear and Plasma Science Society (NPSS) Graduate Scholarship Award for his research on transient plasmas generated by High Power Microwaves (HPM)
5. George Laity was awarded the 2012 graduate directed energy scholarship from the Directed Energy Professional Society.
6. Sterling Beeson, TTU, doctoral student received a scholarship from the Science, Mathematics And Research for Transformation (SMART) Scholarship for Service Program from the Department of Defense.
7. George Laity, doctoral student at TTU, received the Tom Burkes Outstanding Graduate Student Award at the 2012 International Power Modulator and High Voltage Conference.
8. Jonathan Foster received the international IEEE Outstanding Pulsed Power Student Award for 2011.
9. Jacob Stephens and Andrew Fierro, both TTU, received a NPSC (national physical science consortium) graduate student fellowship, a first at Texas Tech University, in 2011. The fellowship is continuing until graduation.
10. George Laity, TTU, received the 2011 Lawrence F. Skibbie Graduate Scholarship from National Defense Industrial Society.

11. Jonathan Foster, TTU, received a National Defense Science and Engineering Graduate Fellowship, 2010 until graduation.
12. George Laity, TTU, has been selected as a NASA/Texas Space Grant Consortium Fellow for the 2010-2011 academic year. Mr. Laity also received a national 2010 graduate fellowship from the Directed Energy Professional Society.

### 6.3 Invited or Award-winning Talks

1. *Invited:* G Laity, A Fierro, L Hatfield, J Dickens, A Neuber, K Frank, "A passive method for determining plasma dissociation degree using vacuum UV self-absorption spectroscopy," presented at the IEEE Pulsed Power & Plasma Science Conference, June 16th-21st, 2013
2. *Invited:* A. Neuber, "Stand-Alone Pulsed Power Generator for HPM Generation," International Conference on Plasma Science, Edinburgh, Scotland, July 8-12, 2012
3. *Invited:* A. Neuber, "Compact Pulsed Power – Dielectric Breakdown," GE Global Research Center, Niskayuna, NY, 2011
4. *Invited:* A. Neuber, "High Power Microwaves – Issues and Challenges", Penn State University, 2011
5. *Invited:* A. Neuber, "Surface Flashover," Pulsed Power School 2010, Mianyang, PR China, July 2010
6. P. Zhang, Y. Y. Lau, and R. S. Timsit, "Spreading Resistance of Contact Spot on a Thin Film", 59th IEEE Holm Conference on Electrical Contacts, Newport, RI USA (September 2013). [Oral]
7. **(Invited Seminar)** Y. Y. Lau, "Effects of Surface Roughness on Electrical Contact, RF Heating and Field Enhancement", Nanyang Technological U, Singapore (5/4/2011); NRL (9/19/2011); UC Davis (10/17/2011); AFOSR (1/9/2012); Rutgers U (2/22/2012); AFRL (6/26/2012); Caltech (10/16/2012); Tsinghua U, Beijing (6/24/2013).
8. **(Invited Seminar)** P. Zhang, "Contact resistance and current crowding in bulk and thin film contacts with dissimilar materials", Electrical and Computer Engineering Seminar Series, Michigan State University, East Lansing, Michigan, 01/30/2014.
9. **(Invited Talk)** P. Zhang, and Y. Y. Lau, "Recent development on the modeling of electrical contact", IEEE Pulsed Power & Plasma Science Conference - PPS 2013 (June 2013, San Francisco, California, USA).
10. **(Invited Talk)** P. Zhang, Y. Y. Lau, and R. M. Gilgenbach, "Bulk and Thin Film Contact Resistance with Dissimilar Materials", The Semiconductor Manufacturing Advanced Process Control (APC) Conference XXIV 2012 (September 2012, Ann Arbor, MI, USA).
11. **(Invited Seminar)** Peng Zhang, "Current Crowding and Constriction Resistance in Bulk and Thin Film Contacts", Microwave Technology Branch Seminar, Naval Research Laboratory, Washington, DC, 04/10/2013.
12. **(Invited Seminar)** P. Zhang, "Current Crowding and Constriction Resistance in Bulk and Thin Film Contacts", Special Seminar, University of Maryland, College Park, MD, 04/11/2013.
13. **(Invited Seminar)** P. Zhang, "Effects of Surface Roughness on Electrical Contact, RF Heating and Field Enhancement", Center for Energy Research, University of California San Diego, La Jolla, CA, 01/2012.

14. Invited Plenary Presentation at PPPS 2013 in San Francisco, CA by Richard Temkin, the IEEE Plasma Science and Applications Award winner invited talk.
15. The IVEC 2012 paper, "1.5 MW, 110 GHz Gyrotron Breakdown in Air," by Jason Hummelt was selected as one of the five finalists for the IVEC 2012 Best Student Paper Award.
16. Verboncoeur, J. P., "PIC Modeling Techniques", Nuclear Physics Institute, Catania, Italy (2009) invited.
17. Verboncoeur, J. P., "Using XOOPIC", Nuclear Physics Institute, Catania Italy (2009), invited.
18. Verboncoeur, J.P., "Computer Experimentation: Particle-in-Cell Simulation of Collisional Plasmas", 19th Int. Symp. Plasma Chem., Bochum, Germany (2009) invited.
19. Lieberman, M.A., E. Kawamura<sup>1</sup>, A.J. Lichtenberg, and J.P. Verboncoeur, "Double layer formation in a two-region electronegative plasma", 19th Int. Symp. Plasma Chem., Bochum, Germany (2009) invited.
20. Verboncoeur, J. P., "Multipactor Breakdown", L3 Communications, San Carlos, CA (2010) invited.
21. Verboncoeur, J. P., "Modeling Plasma Breakdown of Dielectric Windows", Dept. ECE, Michigan State University, East Lansing, MI (2010) invited.
22. Verboncoeur, J. P., "Particle-in-Cell Modeling of Plasmas", Science at the Edge Series, Michigan State University, East Lansing, MI (2010) invited.
23. Verboncoeur, J. P., "Microwave-driven breakdown: from dielectric surface multipactor to ionization discharge", Michigan Institute for Plasma Science and Engineering Colloquium, University of Michigan, Ann Arbor, Michigan (2011) invited
24. Verboncoeur, J. P., "Microwave-driven breakdown", National Superconducting Cyclotron Laboratory/Facility for Rare Isotope Beams Colloquium, Michigan State University, East Lansing, MI (2011) invited
25. Verboncoeur, J. P., "Challenges in plasma modeling", Electromagnetics Seminar Series, Michigan State University, East Lansing, MI (2011) invited
26. Verboncoeur, J. P., "Computational plasma physics and applications", College of Engineering Seminar, Michigan State University, East Lansing, MI (2011) invited.
27. Verboncoeur, J. P., "Kinetic global model for high pressure plasmas", Pusan National University, Busan, South Korea (2013)
28. Verboncoeur, J. P., "Fundamentals of Particle Simulation of Plasmas", Tsinghua University, Beijing, China (2013)
29. Verboncoeur, J. P., "High Voltage Breakdown Physics", Xi'an Jiao Tong University, Xi'an, China (2013)
30. "Vacuum Electronic Sources of High Power Terahertz-Regime Radiation," John H. Booske, **Plenary Talk**, IEEE International Conference on Vacuum Electronics, Bangalore, IN, February 21-25, 2011.

# AFOSR Deliverables Submission Survey

Response ID:3315 Data

1.

---

## 1. Report Type

Final Report

---

## Primary Contact E-mail

Contact email if there is a problem with the report.

booske@engr.wisc.edu

---

## Primary Contact Phone Number

Contact phone number if there is a problem with the report

608-890-0804

---

## Organization / Institution name

University of Wisconsin-Madison

---

## Grant/Contract Title

The full title of the funded effort.

BASIC STUDIES OF DISTRIBUTED DISCHARGE LIMITERS FOR COUNTER-HPM

---

## Grant/Contract Number

AFOSR assigned control number. It must begin with "FA9550" or "F49620" or "FA2386".

FA9550-09-1-0086

---

## Principal Investigator Name

The full name of the principal investigator on the grant or contract.

Professor John H. Booske

---

## Program Manager

The AFOSR Program Manager currently assigned to the award

Dr. John Luginsland

---

## Reporting Period Start Date

03/01/2009

---

## Reporting Period End Date

11/30/2013

---

## Abstract

We completed a comprehensive research investigation on distributed, self-initiated plasma discharges as candidate deployable surfaces providing counter-HPM capabilities. The study revealed how to control and accelerate breakdown using: (1) DC voltage bias effects and seed electron sources including radioactive sources, prior breakdown discharges, UV pre-excitation/pre-ionization, VUV radiation, multipactor, and field or triple-point emission; (2) optimization of neutral gas pressure (1-760 torr) and collisionality effects and gas species (noble gases, air, and Penning gas mixtures); and (3) Metamaterials and metasurfaces. Coordinated experimental and modeling studies characterized and revealed new physical understanding of plasma

DISTRIBUTION A: Distribution approved for public release.

filamentation, non-thermal electron energy distribution functions (EEDFs), and post-pulse recovery. Advanced experimental capabilities were developed and are ripe for exploitation for further research including: (1) methods to apply DC field bias along with intense microwave fields to window surfaces; (2) methods to exploit metasurfaces and metamaterials for enhanced control of timing and spatial distribution of breakdown; (3) microwave reflection, transmission, and scattering and CCD camera imaging diagnostics to extract rapidly varying properties of highly localized plasmas in the presence of intense HPM fields; (4) advanced OES diagnostics to extract gas and plasma temperatures, plasma densities, and non-Maxwellian EEDFs, (5) precise gas mixture control (e.g., Penning gas mixtures); and (6) seed electron source production. Advanced time-dependent multi-physics theoretical modeling capabilities were developed and are ripe for exploitation in further research of phenomena such as triple-point emission, multipactor breakdown, high pressure gas collisional discharge breakdown, field emission (including space charge limits), statistics of seed electron production, high pressure plasma filamentation, DC electric bias field effects, and electrical junction heating and electro-thermal runaway physics. Scholarship completed and recognitions acquired during the grant included 54 journal publications, 129 conference papers/presentations, and 9 prestigious awards/honors bestowed on 3 faculty with an additional 12 awards/honors for students/staff, complemented by 30 invited or award-winning talks. 48 grad students or post-docs, 8 undergrad students, and 26 faculty and staff were involved in the research sponsored in part or entirely by this grant.

---

**Distribution Statement**

This is block 12 on the SF298 form.

Distribution A - Approved for Public Release

---

**Explanation for Distribution Statement**

If this is not approved for public release, please provide a short explanation. E.g., contains proprietary information.

---

**SF298 Form**

Please attach your SF298 form. A blank SF298 can be found [here](#). Please do not spend extra effort to password protect or secure the PDF, we want to read your SF298. The maximum file size for SF298's is 50MB.

[Final Report Cover page.pdf](#)

---

**Upload the Report Document. The maximum file size for the Report Document is 50MB.**

[CHPM I Final Report final.pdf](#)

---

**Upload a Report Document, if any. The maximum file size for the Report Document is 50MB.**

---

**Archival Publications (published) during reporting period:**

Far too many to cut and paste here. See report for complete list.

---

**Changes in research objectives (if any):**

None

---

**Change in AFOSR Program Manager, if any:**

None

---

**Extensions granted or milestones slipped, if any:**

None

---

**AFOSR LRIR Number**

---

**LRIR Title**

---

**Reporting Period**

## Laboratory Task Manager

### Program Officer

### Research Objectives

### Technical Summary

### Funding Summary by Cost Category (by FY, \$K)

	Starting FY	FY+1	FY+2
Non-Military Government Personnel Costs			
In-house Contractor Costs			
Travel (Be Specific)			
Training (Be Specific)			
Supplies			
Other Expenses (Be Specific)			
Total Resource Requirements			

### Report Document

### Appendix Documents

## 2. Thank You

---

### E-mail user

Feb 10, 2014 13:01:04 Success: Email Sent to: booske@engr.wisc.edu

Response ID: 3315

<b>Survey Submitted:</b>	Feb 10, 2014 (1:01 PM)
<b>IP Address:</b>	144.92.105.92
<b>Language:</b>	English (en-US,en;q=0.5)
<b>User Agent:</b>	Mozilla/5.0 (Windows NT 6.1; WOW64; rv:26.0) Gecko/20100101 Firefox/26.0
<b>Http Referrer:</b>	
<b>Page Path:</b>	1 : (SKU: 1) 2 : Thank You (SKU: 2)
<b>SessionID:</b>	1392053451_52f90ccb5749d1.27677637

Response Location

<b>Country:</b>	United States DISTRIBUTION A: Distribution approved for public release.
-----------------	--

<b>Region:</b>	WI
<b>City:</b>	Madison
<b>Postal Code:</b>	53706
<b>Long &amp; Lat:</b>	Lat: 43.076099, Long:-89.4104